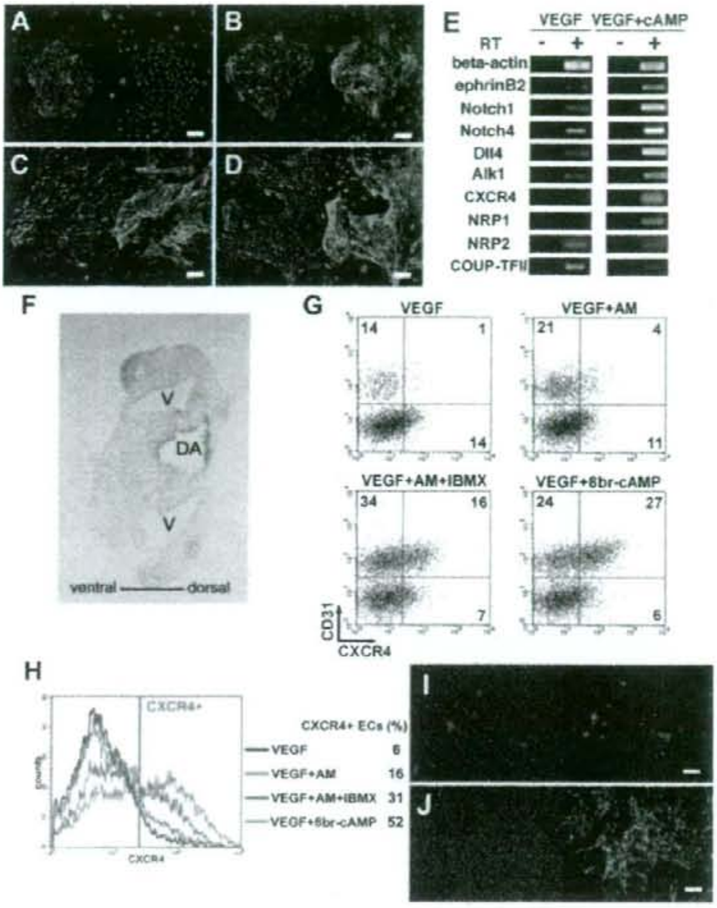

Figure 2. The effect of AM and cAMP on arterial EC induction from VEGFR2^{+} cells. A to D, Double fluorescent staining for CD31 and ephrinB2 after 3 days of culture of VEGFR2^{+} cells. Left panels, CD31 (pan-ECs, red) and DAPI (blue). Right panels, EphB4-Fc (ephrinB2^{+} arterial ECs, green) and DAPI (blue). A, VEGF treatment alone (50 ng/mL). B, VEGF with 10^{-6} mol/L AM. C, VEGF with 10^{-6} mol/L AM and 10^{-4} mol/L IBMX. D, VEGF with 0.5 mmol/L 8bromo-cAMP. Scale bars: 100 μm. E, Reverse-transcription polymerase chain reaction showing mRNA expression of arterial markers (ephrinB2, Notch1, Notch4, Dll4, Alk1, CXCR4, and NRP1) and venous marker (NRP2 and COUP-TFII) in purified ECs induced by VEGF treatment alone or VEGF and 8bromo-cAMP treatment. F, Aortic EC-specific expression of CXCR4 (purple) by in situ hybridization of the isolated aorta-gonad-mesonephros (AGM) region in E11.5 mouse embryo. DA indicates dorsal aorta; V, Cardinal veins. G, Flow cytometry for CD31 and CXCR4 expression. Left upper panel, VEGF treatment alone (50 ng/mL). Right upper panel, VEGF with 10^{-6} mol/L AM. Left lower panel, VEGF with 10^{-6} mol/L AM and 10^{-4} mol/L IBMX. Right lower panel, VEGF with 0.5 mmol/L 8bromo-cAMP. H, Expression profile of CXCR4 in CD31^{+} ECs by flowcytometry. VEGF treatment alone (blue line), VEGF with 10^{-6} mol/L AM (green line), VEGF with 10^{-6} mol/L AM and 10^{-4} mol/L IBMX (red line), and VEGF with 0.5mmol/L 8bromo-cAMP (orange line) are shown. Percentages of CXCR4^{+} arterial ECs in total ECs are indicated. I and J, Gross appearance of ephrinB2^{+} arterial EC induction from VEGFR2^{+} cells (plated at 2×10^{4} cells/cm^{2}). Left panels, DAPI (blue). Right panels, EphB4-Fc (ephrinB2^{+} arterial ECs, green). I, VEGF treatment alone (50 ng/mL). J, VEGF with 0.5 mmol/L 8bromo-cAMP. Increase in cell number (DAPI) and substantial arterial EC induction were observed. Scale bars: 400 μm.

8bromo-cAMP and VEGF treatment (Figure 2E). These results indicated that stimulation of cAMP pathway induces arterial ECs.

We further attempted to quantitatively evaluate arterial EC induction at the cellular level. CXCR4, a 7-transmembrane G-protein-coupled receptor, is the receptor of CXCL12 (also known as stromal cell-derived factor-1). Recently, CXCR4 has been reported to be expressed in ECs in the superior mesenteric artery, but not in the superior mesenteric vein, and involved in the formation of arteries in the gastrointestinal tract.[29,30] We examined CXCR4 expression in the mouse embryo by in situ hybridization and found that CXCR4 was detected in ECs of the dorsal aorta but not of cardinal veins in aorta-gonado-mesonephros (AGM) region of E11.5 embryos (Figure 2F). In addition, mRNA expression of CXCR4 was increased in 8bromo-cAMP and VEGF-treated ECs together with other arterial EC markers (Figure 2E), indicating that CXCR4 is another arterial EC marker. FACS analysis using an anti-CXCR4 antibody successfully quantified arterial EC induction by AM or 8bromo-cAMP treatment. Most of ECs induced by VEGF treatment alone (>90% to 95%) were negative for CXCR4. CXCR4^{+}/CD31^{+} arterial ECs were induced in the presence of AM together with VEGF. Addition of AM with IBMX, or 8bromo-cAMP further increased CXCR4^{+}/CD31^{+} arterial EC appearance (Figure 2G). Overall, 8bromo-cAMP and VEGF treatment induced ≈5- to 10-fold more CXCR4^{+} arterial ECs compared with VEGF treatment alone. AM with VEGF treatment showed slight effect on the arterial EC induction. Simultaneous administration of AM and IBMX with VEGF enhanced the arterializing effect of AM (Figure 2H). These results indicated that cAMP signaling mainly contributes to the arterial EC induction. The maximum percentage of arterial ECs within total ECs was increased to ≈60% by 8bromo-cAMP and VEGF (Figure 3F). Addition of 8bromo-cAMP with VEGF led to an increase in total cell number, total EC number, and arterial EC percentage, resulting in ≈70-times increment of induced arterial EC number than those by VEGF alone (Figure 2I and 2J). Higher doses of VEGF (100 to 200 ng/mL) alone or 8bromo-cGMP (0.5 mmol/L) with VEGF

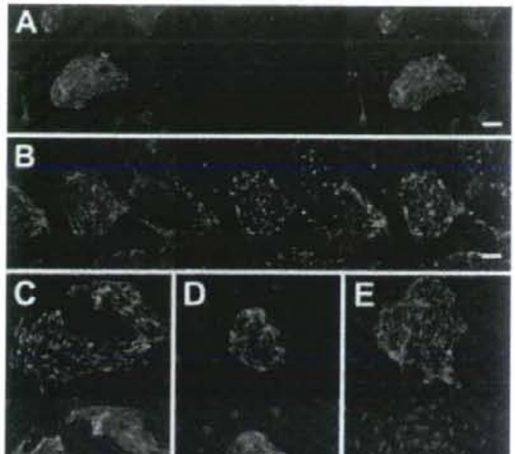

Figure 3. Essential role of Notch signaling in arterial EC induction. A and B, Double fluorescent staining of cleaved Notch intracellular domain (NICD) and CD31 for induced ECs. Left panels, CD31 (pan-ECs, red). Middle panels, Cleaved NICD (green). Right panels, Merged image. A, VEGF treatment alone (50 ng/mL). B, VEGF with 0.5 mmol/L 8bromo-cAMP. Scale Bars: 200 μm. C to E, Double-fluorescent staining of CD31 and ephrinB2 for ECs induced by VEGF with 8bromo-cAMP using RBP-J–deficient ES cells. Upper panels, CD31 (pan-ECs, red) and DAPI (blue). Lower panels, EphB4-Fc (ephrinB2^{+} arterial ECs, green) and DAPI (blue). C, RBP-J$^{+/+}$ ES cells. D, RBP-J$^{+/-}$ ES cells. E, RBP-J$^{-/-}$ ES cells. Scale bars: 100 μm. F and G, Expression profile of CXCR4 in CD31^{+} ECs. F, Blue and green lines: RBP-J$^{+/+}$ cells. VEGF treatment alone (blue line), VEGF with 0.5 mmol/L 8bromo-cAMP (green line). Red and orange lines: RBP-J$^{-/-}$ cells. VEGF alone (red line), VEGF with 0.5 mmol/L 8bromo-cAMP (orange line). Percentages of CXCR4^{+} arterial ECs in total ECs are indicated. G, RBP-J$^{+/+}$ cells. VEGF treatment alone (blue line), VEGF with 0.5 mmol/L 8bromo-cAMP (green line). VEGF with 8bromo-cAMP and 2.5 μmol/L DAPT (red line).

Single-Cell Analysis of VEGFR2^{+} Cell Culture

	VEGF Alone	VEGF With 8bromo-cAMP
Total colony, n (per every 100 sequential wells)	5.62±1.74 (n=16)	16.0±6.06 (n=11)*
EC-including colony, n (per every 10 sequential colonies)	3.40±2.20 (n=15)	7.00±1.70 (n=19)*
AEC-including colony, n (per every 10 sequential colonies)	1.27±1.10 (n=15)	3.63±1.30 (n=19)*
AEC number (per each AEC-including colony)	1.69±0.87 (n=16)	4.51±2.77 (n=76)*

*$P<0.01$ vs VEGF alone.

AEC indicates arterial endothelial cell; EC, endothelial cell.

treatment did not show arterial EC induction. Administration of iloprost (10^{-7} to 10^{-5} mol/L), an analogue of prostaglandin-I2 that elevates intracellular cAMP in mature ECs, showed almost no arterial inducing effect even with VEGF treatment (data not shown). These results indicated that AM/cAMP signaling is a novel potent and specific inducer of arterial ECs from vascular progenitor cells.

To further evaluate the mechanism of AM/cAMP-stimulated arterial EC induction, we performed single-cell culture of VEGFR2^{+} cells. Colonies obtained from single VEGFR2^{+} cells were counted and evaluated by staining for CD31, ephrinB2, and DAPI (Table). VEGF and 8bromo-cAMP treatment significantly increased the total number of colonies that appeared, number of EC-including colonies, and arterial EC-including colonies in appeared colonies, and arterial EC numbers in each arterial EC-including colony than VEGF alone. These results suggest that cAMP increased survival of VEGFR2^{+} progenitor cells, differentiation of ECs and arterial ECs from progenitor cells that survived, and proliferation of arterial ECs. cAMP, thus, should be involved in multi steps of arterial EC differentiation processes.

We then examined the role of Notch signaling in arterial EC induction in this system. Activation of Notch on ligand binding is accompanied by proteolytic processing that releases intracellular domain of Notch (NICD) from the membrane. The NICD then translocates into the nucleus and associates with RBP-J, a DNA-binding protein, to form a transcriptional activator, which turns on transcription of a set of target genes.[31] First, we examined Notch activation by cAMP treatment with immunostaining of cleaved NICD. Whereas Notch signal was not activated in most of ECs induced by VEGF alone (Figure 3A), administration of 8bromo-cAMP together with VEGF clearly induced nuclear localization of cleaved NICD in ECs, indicating that stimulation of cAMP pathway can activate Notch signaling in differentiating ECs (Figure 3B). cAMP is, thus, found to be a novel signaling pathway that interacts with and activates Notch signaling in EC lineages. Then, we performed a loss-of-function study using RBP-J–deficient ES cells that lack Notch signaling activation.[20] VEGFR2^{+} cells derived from RBP-J$^{+/+}$, RBP-J$^{+/-}$, or RBP-J$^{-/-}$ ES cells were sorted and re-cultured with VEGF in the presence of 8bromo-cAMP. Arterial EC induction observed in RBP-J$^{+/+}$ (Figure 3C) or RBP-J$^{+/-}$ ES cells (Figure 3D) was completely abolished in RBP-J$^{-/-}$ ES cells (Figure 3E). FACS analysis using CXCR4 further demonstrated that induction of CXCR4^{+} arterial ECs observed in RBP-J$^{+/-}$ was completely abolished in RBP-J$^{-/-}$ ES cells (Figure 3F). Similarly, administration of γ-secretase inhibitor, DAPT (2.5μmol/L), which inhibits proteolytic processing of Notch to activate its signaling, to VEGFR2^{+} cell culture also completely blocked the arterial EC induction (Figure 3G). These results indicate that Notch signaling is essential for arterial EC induction in this ES cell system, and correlates with previous reports in zebrafish[32,33] and mouse[34,35] genetic animal models.

Next, we examined the effect of a gain-of-function of Notch in arterial EC induction. We used an ES cell line NERT$^{\Delta OP}$-7,[21] in which signaling of the activated intracellular domain of murine Notch1 can be regulated using an OHT-inducible system.[22] NERT$^{\Delta OP}$-7 ES cell-derived VEGFR2^{+} cells were sorted and re-cultured with VEGF in the presence or absence of OHT. In the absence of OHT, NERT protein was located mainly in the cytoplasm of induced CD31^{+} ECs and other cell types (supplemental Figure IA, available online at http://atvb.ahajournals.org). After addition of OHT, NERT protein translocated to the nucleus (supplemental Figure IB). Notch signal activation in VEGF-induced ECs was evaluated by FACS using NERT$^{\Delta OP}$-7/Hes-GFP cells carrying HES promoter-driven GFP gene (supplemental Figure IC). Addition of 8bromo-cAMP induced endogenous Notch activation in ECs, correlating with our previous results shown in Figure 3A and 3B. OHT treatment showed stronger Notch signal activation through NERT protein than 8bromo-cAMP treatment. Simultaneous stimulation by 8bromo-cAMP and OHT additionally enhanced Notch activation in induced ECs. These results indicate that NERT$^{\Delta OP}$-7 cell system can successfully induce Notch signal activation in differentiating ES cells. NERT$^{\Delta OP}$-7 cell-derived ECs induced by VEGF alone were negative for ephrinB2 (Figure 4A). Unexpectedly, hardly any arterial ECs appeared after Notch activation with OHT, even when co-stimulated with VEGF (Figure 4B). Although ephrin-B2^{+} arterial ECs were successfully induced by VEGF with 8bromo-cAMP (Figure 4C), no apparent effect of OHT was observed on the cAMP-stimulated arterial EC induction with ephrinB2 staining (Figure 4D). FACS analysis further demonstrated that activation of Notch signaling by OHT failed to induce CXCR4^{+} arterial ECs and, moreover, activation of Notch signaling with OHT did not affect, or often reduced, cAMP-induced CXCR4^{+} arterial EC induction (Figure 4E). These results indicate that Notch signal is not sufficient or at least aberrant activation of Notch is not beneficial, for arterial EC induction. This is compatible with the previous in vivo study using activated Notch4-transgenic mice in that activation of Notch signaling in embryonic endothelium led to disorganized vascular networks but did not document arterial induction.[36]

Taken together, VEGF appears essential for EC differentiation from VEGFR2^{+} cells, and venous ECs can be induced by VEGF alone. For arterial EC induction, however, VEGF

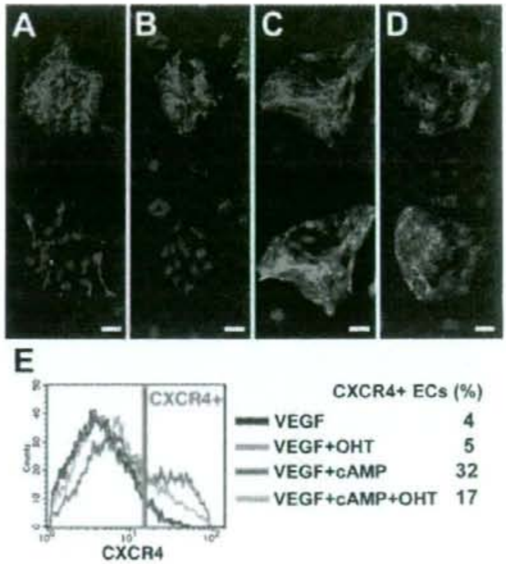

Figure 4. Effects of activated Notch on arterial EC induction from VEGFR2^{+} cells. A-D, Double-fluorescent staining of CD31 and ephrinB2 for induced ECs using NERT$^{\Delta OP}$-7 ES cells. Upper panels, CD31 (pan-ECs, red) and DAPI (blue). Lower panels, EphB4-Fc (ephrinB2^{+} arterial ECs, green) and DAPI (blue). A, VEGF treatment alone (50 ng/mL). B, VEGF and 150 nmol/L OHT. C, VEGF and 0.5 mmol/L 8bromo-cAMP. D, VEGF, 0.5mmol/L 8bromo-cAMP, and 150 nmol/L OHT. Scale bars: 100 μm. E, Expression profile of CXCR4 in CD31^{+} ECs. VEGF alone (blue line), VEGF and OHT (green line), VEGF and 8bromo-cAMP (red line), and VEGF, 8bromo-cAMP, and OHT (orange line) are shown. Percentages of CXCR4^{+} arterial ECs in total ECs are indicated.

and Notch signaling is essential but not sufficient. AM/cAMP pathway can activate Notch signaling, and is another important signaling to induce arterial ECs. Coordinated signaling of VEGF, Notch, and cAMP is the combination that composes a sufficient condition to constructively induce arterial ECs from vascular progenitor cells.

Discussion

Our findings provide the first demonstration to our knowledge of arterial and venous EC induction from ES cells by constructively reproducing endothelial differentiation processes in vitro. Here we showed that cAMP and AM play specific roles in EC differentiation, especially for arterial EC induction, from VEGFR2^{+} vascular progenitors. We have shown that AM enhances proliferation and migration of cultured ECs and can promote angiogenesis in gel plug assays in vivo.[37] Recently, AM was reported to enhance angiogenic potency of bone marrow cell transplantation.[38] AM should be a novel potent candidate for an endogenous ligand for EC differentiation as well as arterial EC induction.

Our results showed that stimulation of cAMP pathway can activate Notch signaling in EC lineage. To date, little evidence of Notch activation by cAMP pathway has been reported. In neuronal cells, cAMP-response element-binding protein increased expression of presenilin-1, a component of

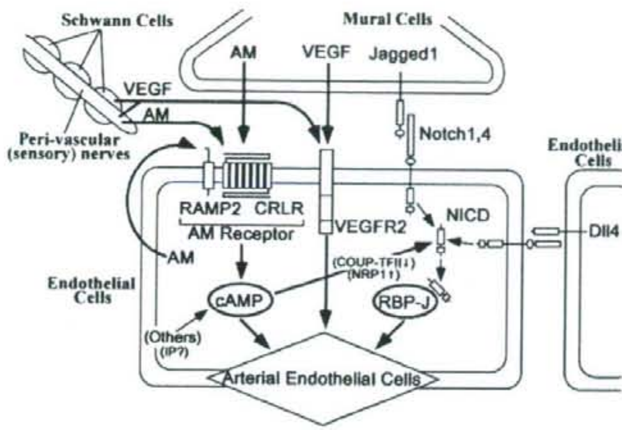

Figure 5. Cellular and molecular mechanisms of arterial EC induction. Putative autocrine/paracrine system for arterial induction in vascular wall. Signals for arterial induction, VEGF, Notch, and AM/cAMP components exist in the vascular wall. VEGFR2, AM receptor complex, RAMP2 and CRLR, and Notch1 and 4 are expressed in ECs. However, their ligands, VEGF, AM, and Jagged1 are expressed in mural cells (MCs). Moreover, AM is expressed in ECs and perivascular nerves. VEGF is produced from peripheral sensory nerves and Schwann cells. Notch ligands, Dll4, and Jagged1 are expressed in arterial ECs. These autocrine/paracrine signals among ECs, MCs, and other perivascular tissues should coordinately regulate the arterial induction and maintenance.

γ-secretase, through transcriptional activation.[39] A similar mechanism may contribute in EC and EC progenitors to induce Notch activation. Recently, COUP-TFII has been reported to repress Notch signaling through suppressing NRP1 expression to maintain vein identity.[28] Administration of 8bromo-cAMP did not increase mRNA expression of Notch ligands (ie, jagged1, 2, Delata-like1, 3, 4) in surrounding mural cells (data not shown), but suppressed COUP-TFII and increased NRP1 expression in ECs. These results suggest that cAMP pathway may activate Notch signaling through the suppression of COUP-TFII expression. cAMP pathway, thus, may regulate the determination of cell fates between arterial and venous ECs. Although Dll4 and Notch signaling were reported to be growth-suppressive on mature ECs through downregulation of VEGFR2 and NRP1 expression,[40] forced Notch activation with OHT did not affect on VEGFR2 and NRP1 mRNA expression in differentiating ECs (data not shown). Notch signaling may possess differentiation stage-specific roles in EC differentiation and proliferation. Precise molecular interactions among these pathways should be further investigated to figure out the whole scheme of arterial-venous specification.

In the vascular wall, VEGFR2, Notch1 and 4, and AM receptor complex, CRLR, RAMP-2 and -3, are expressed in ECs.[5,6] On the other hand, their ligands, VEGF, Jagged1, and AM, are expressed in MCs.[8,41,42] Dll4 and AM are also expressed in ECs. We confirmed AM mRNA expression in ES cell-derived ECs and MCs, and RAMP-2 and CRLR mRNA in ECs by reverse-transcription polymerase chain reaction analysis. Low-level expression of prostaglandin-I2 receptor mRNA was also observed in ECs (data not shown). Moreover, peripheral sensory nerve and Schwann cell-derived VEGF are reported to be involved in arterial EC induction.[43] AM is demonstrated to be expressed in perivascular nerves in the rat mesenteric artery.[44] The autocrine/paracrine cross-talk of VEGF, Notch, and AM/cAMP signaling between ECs and MCs, and signals from other perivascular tissues, should coordinately regulate vascular development including the induction and maintenance of the arterial structures (Figure 5). Combinatory signaling of VEGF, Notch, and cAMP may mimic these arterial-inducing machineries in vivo to achieve constructive induction of arterial ECs from vascular progenitor cells in vitro.

Our constructive approach has successfully provided a novel understanding for the mechanisms of arterial EC differentiation. This study, thus, would provide a potent novel strategy as constructive developmental biology to dissect cell differentiation processes and contribute to regenerative medicine.

Acknowledgments

We thank Dr Ohtsuka and Dr Kagayama for Hes promoter gene constructs. We also thank Drs Takahashi and Hoshino for critical reading of the manuscript.

Sources of Funding

J.K.Y. is supported by grants from the Ministry of Education, Science, Sports, and Culture of Japan, the Ministry of Health, Labor, and Welfare of Japan, and PRESTO JST. U.J. is supported by the Deutsche Forschungsgemeinschaft Priority Program 1109 "Stem Cells" and Sonderforschungsbereich 415 "Signal transduction."

Disclosures

None.

References

1. Carmeliet P. Mechanisms of angiogenesis and arteriogenesis. *Nat Med.* 2000;6:389–395.
2. Sato TN. Vascular development: molecular logic for defining arteries and veins. *Curr Opin Hematol.* 2003;10:131–135.
3. Wang HU, Chen ZF, Anderson DJ. Molecular distinction and angiogenic interaction between embryonic arteries and veins revealed by ephrin-B2 and its receptor Eph-B4. *Cell.* 1998;93:741–753.
4. Adams RH, Wilkinson GA, Weiss C, Diella F, Gale NW, Deutsch U, Risau W, Klein R. Roles of ephrinB ligands and EphB receptors in cardiovascular development: demarcation of arterial/venous domains, vascular morphogenesis, and sprouting angiogenesis. *Genes Dev.* 1999;13:295–306.
5. Lawson ND, Weinstein BM. Arteries and veins: making a difference with zebrafish. *Nat Rev Genet.* 2002;3:674–682.
6. Yamashita JK. Differentiation and diversification of vascular cells from embryonic stem cells. *Int J Hematol.* 2004;80:1–6.
7. Rossant J, Hirashima M. Vascular development and patterning: making the right choices. *Curr Opin Genet Dev.* 2003;13:408–412.
8. Shawber CJ, Kitajewski J. Notch function in the vasculature: insights from zebrafish, mouse and man. *Bioessays.* 2004;26:225–234.

9. Zhong TP, Rosenberg M, Mohideen MA, Weinstein B, Fishman MC. gridlock, an HLH gene required for assembly of the aorta in zebrafish. *Science*. 2000;287:1820–1824.
10. Fischer A, Schumacher N, Maier M, Sendtner M, Gessler M. The Notch target genes Hey1 and Hey2 are required for embryonic vascular development. *Genes Dev*. 2004;18:901–911.
11. Daniel PB, Walker WH, Habener JF. Cyclic AMP signaling and gene regulation. *Annu Rev Nutr*. 1998;18:353–383.
12. Kitamura K, Kangawa K, Kawamoto M, Ichiki Y, Nakamura S, Matsuo H, Eto T. Adrenomedullin: a novel hypotensive peptide isolated from human pheochromocytoma. *Biochem Biophys Res Commun*. 1993;192:553–560.
13. McLatchie LM, Fraser NJ, Main MJ, Wise A, Brown J, Thompson N, Solari R, Lee MG, Foord SM. RAMPs regulate the transport and ligand specificity of the calcitonin-receptor-like receptor. *Nature*. 1998;393:333–339.
14. Shimosawa T, Ogihara T, Matsui H, Asano T, Ando K, Fujita T. Deficiency of adrenomedullin induces insulin resistance by increasing oxidative stress. *Hypertension*. 2003;41:1080–1085.
15. Shindo T, Kurihara Y, Nishimatsu H, Moriyama N, Kakoki M, Wang Y, Imai Y, Ebihara A, Kuwaki T, Ju KH, Minamino N, Kangawa K, Ishikawa T, Fukuda M, Akimoto Y, Kawakami H, Imai T, Morita H, Yazaki Y, Nagai R, Hirata Y, Kurihara H. Vascular abnormalities and elevated blood pressure in mice lacking adrenomedullin gene. *Circulation*. 2001;104:1964–1971.
16. Caron KM, Smithies O. Extreme hydrops fetalis and cardiovascular abnormalities in mice lacking a functional adrenomedullin gene. *Proc Natl Acad Sci U S A*. 2001;98:615–619.
17. Nishikawa SI, Nishikawa S, Hirashima M, Matsuyoshi N, Kodama H. Progressive lineage analysis by cell sorting and culture identifies FLK1+VE-cadherin+ cells at a diverging point of endothelial and hemopoietic lineages. *Development*. 1998;125:1747–1757.
18. Yamashita J, Itoh H, Hirashima M, Ogawa M, Nishikawa S, Yurugi T, Naito M, Nakao K, Nishikawa SI. Flk1-positive cells derived from embryonic stem cells serve as vascular progenitors. *Nature*. 2000;408:92–96.
19. Yurugi-Kobayashi T, Itoh H, Yamashita J, Yamahara K, Hirai H, Kobayashi T, Ogawa M, Nishikawa S, Nishikawa SI, Nakao K. Effective contribution of transplanted vascular progenitor cells derived from embryonic stem cells to adult neovascularization in proper differentiation stage. *Blood*. 2003;101:2675–2678.
20. Schroeder T, Fraser M, Ogawa M, Nishikawa S, Oka C, Bornkamm GW, Nishikawa SI, Honjo T, Just U. Recombination signal sequence-binding protein Jkappa alters mesodermal cell fate decisions by suppressing cardiomyogenesis. *Proc Natl Acad Sci U S A*. 2003;100:4018–4023.
21. Schroeder T, Meier-Stiegen F, Schwanbeck R, Eilken H, Nishikawa S, Haler R, Schreiber S, Bornkamm GW, Nishikawa SI, Just U. Activated Notch1 alters differentiation of embryonic stem cells into mesodermal cell lineages at multiple stages of development. *Mech Dev*. In press.
22. Schroeder T, Just U. Notch signalling via RBP-J promotes myeloid differentiation. *EMBO J*. 2000;19:2558–2268.
23. Ohtsuka T, Imayoshi I, Shimojo H, Nishi E, Kageyama R, McConnell SK. Visualization of embryonic neural stem cells using Hes promoters in transgenic mice. *Mol Cell Neurosci*. doi 10.1016/j.mcn. 2005.09.006.
24. Yamashita JK, Takano M, Hiraoka-Kanie M, Shimazu C, Peishi Y, Yanagi K, Nakano A, Inoue E, Kita F, Nishikawa SI Prospective identification of cardiac progenitors by a novel single cell-based cardiomyocyte induction. *FASEB J*. 2005;19:1534–1536.
25. Ara T, Tokoyoda K, Okamoto R, Pandelakis AK, Nagasawa T. The role of CXCL12 in the organ-specific process of artery formation. *Blood*. 2005;105:3155–3161.
26. Hippenstiel S, Witzenrath M, Schmeck B, Hocke A, Krisp M, Krüll M, Seybold J, Seeger W, Rascher W, Schütte H, Suttorp N. Adrenomedullin reduces endothelial hyperpermeability. *Circ Res*. 2002;91:618–625.
27. Fuller T, Korff T, Kilian A, Dandekar G, Augustin HG. Forward EphB4 signaling in endothelial cells controls cellular repulsion and segregation from ephrinB2 positive cells. *J Cell Sci*. 2003;116:2461–2470.
28. You LR, Lin FJ, Lee CT, DeMayo FJ, Tsai MJ, Tsai SY. Suppression of Notch signaling by the COUP-TFII transcription factor regulates vein identity. *Nature*. 2005;435:98–104.
29. Herzog Y, Guttmann-Raviv N, Neufeld G. Segregation of arterial and venous markers in subpopulations of blood islands before vessel formation. *Dev Dyn*. 2005;232:1047–1055.
30. Tachibana K, Hirota S, Iizasa H, Yoshida H, Kawbata K, Kataoka Y, Kitamura Y, Matsushima K, Yoshida N, Nishikawa SI, Kishimoto T, Nagasawa T. The chemokine receptor CXCR4 is essential for vascularization of the gastrointestinal tract. *Nature*. 1998;393:591–594.
31. Mumm JS, Kopan R. Notch signaling: from the outside in. *Dev Biol*. 2000;228:151–165.
32. Zhong TP, S. Childs, J.P. Leu, Fishman. MC. Gridlock signalling pathway fashions the first embryonic artery. *Nature*. 2001;414:216–220.
33. Lawson ND, Scheer N, Pham VN, Kim CH, Chitnis AB, Campos-Ortega JA, Weinstein BM. Notch signaling is required for arterial-venous differentiation during embryonic vascular development. *Development*. 2001;128:3675–3683.
34. Duarte A, Hirashima M, Benedito R, Trindade A, Diniz P, Bekman E, Costa L, Henrique D, Rossant J. Dosage-sensitive requirement for mouse Dll4 in artery development. *Genes Dev*. 2004;18:2474–2478.
35. Krebs LT, Shutter JR, Tanigaki K, Honjo T, Stark KL, Gridley T. Haploinsufficient lethality and formation of arteriovenous malformations in Notch pathway mutants. *Genes Dev*. 2004;18:2469–2473.
36. Uyttendaele H, Ho J, Rossant J, Kitajewski J. Vascular patterning defects associated with expression of activated Notch4 in embryonic endothelium. *Proc Natl Acad Sci U S A*. 2001;98:5643–5648.
37. Miyashita K, Itoh H, Sawada N, Fukunaga Y, Sone M, Yamahara K, Yurugi-Kobayashi T, Park K, Nakao K. Adrenomedullin provokes endothelial Akt activation and promotes vascular regeneration both in vitro and in vivo. *FEBS Lett*. 2003;544:86–92.
38. Iwase T, Nagaya N, Fujii T, Itoh T, Ishibashi-Ueda H, Yamagishi M, Miyatake K, Matsumoto T, Kitamura S, Kangawa K. Adrenomedullin enhances angiogenic potency of bone marrow transplantation in a rat model of hindlimb ischemia. *Circulation*. 2005;111:356–362.
39. Mitsuda N, Ohkubo N, Tamatani M, Lee YD, Taniguchi M, Namikawa K, Kiyama H, Yamaguchi A, Sato N, Sakata K, Ogihara T, Vitek MP, Tohyama M. Activated cAMP-response element-binding protein regulates neuronal expression of presenilin-1. *J Biol Chem*. 2001;276:9688–9698.
40. Williams CK, Li JL, Murga M, Harris AL, Tosato G. Up-regulation of the Notch ligand Delta-like 4 inhibits VEGF-induced endothelial cell function. *Blood*. 2006;107:931–939.
41. Darland DC, Massingham LJ, Smith SR, Piek E, Saint-Geniez M, D'Amore PA. Pericyte production of cell-associated VEGF is differentiation-dependent and is associated with endothelial survival. *Dev Biol*. 2003;264:275–288.
42. Montuenga LM, Mariano K, Prentice MA, Cuttitta F, Jakowlew SB. Coordinate expression of transforming growth factor-beta1 and adrenomedullin in rodent embryogenesis. *Endocrinology*. 1998;139:3946–3957.
43. Mukouyama YS, Shin D, Britsch S, Taniguchi M, Anderson DJ. Sensory nerves determine the pattern of arterial differentiation and blood vessel branching in the skin. *Cell*. 2002;109:693–705.
44. Hobara N, Nakamura A, Ohtsuka A, Narasaki M, Shibata K, Gomoita Y, Kawasaki H. Distribution of adrenomedullin-containing perivascular nerves in the rat mesenteric artery. *Peptides*. 2004;25:589–599.

0013-7227/06/$15.00/0
Printed in U.S.A.

Endocrinology 147(4):1642–1653

doi: 10.1210/en.2005-1038

The Neuroprotective and Vasculo-Neuro-Regenerative Roles of Adrenomedullin in Ischemic Brain and Its Therapeutic Potential

Kazutoshi Miyashita, Hiroshi Itoh, Hiroshi Arai, Takayasu Suganami, Naoki Sawada, Yasutomo Fukunaga, Masakatsu Sone, Kenichi Yamahara, Takami Yurugi-Kobayashi, Kwijun Park, Naofumi Oyamada, Naoya Sawada, Daisuke Taura, Hirokazu Tsujimoto, Ting-Hsing Chao, Naohisa Tamura, Masashi Mukoyama, and Kazuwa Nakao

Department of Medicine and Clinical Science (K.M., H.I., H.A., N.S., Y.F., M.S., K.Y., T.Y.-K., K.P., N.O., N.S., D.T., H.T., N.T., M.M., K.N.), Kyoto University Graduate School of Medicine, Kyoto 606-8507, Japan; Department of Molecular Medicine and Metabolism (T.S.), Medical Research Institute, Tokyo Medical and Dental University, Tokyo 101-0062, Japan; and Department of Medicine (T.-H.C.), National Cheng-Kung University Medical Center, Tainan, Taiwan 701, Republic of China

Adrenomedullin (AM) is a vasodilating hormone secreted mainly from vascular wall, and its expression is markedly enhanced after stroke. We have revealed that AM promotes not only vasodilation but also vascular regeneration. In this study, we focused on the roles of AM in the ischemic brain and examined its therapeutic potential. We developed novel AM-transgenic (AM-Tg) mice that overproduce AM in the liver and performed middle cerebral artery occlusion for 20 min (20m-MCAO) to examine the effects of AM on degenerative or regenerative processes in ischemic brain. The infarct area and gliosis after 20m-MCAO was reduced in AM-Tg mice in association with suppression of leukocyte infiltration, oxidative stress, and apoptosis in the ischemic core. In addition, vascular regeneration and subsequent neurogenesis were enhanced in AM-Tg mice, preceded by increase in mobilization of $CD34^+$ mononuclear cells, which can differentiate into endothelial cells. The vasculo-neuro-regenerative actions observed in AM-Tg mice in combination with neuroprotection resulted in improved recovery of motor function. Brain edema was also significantly reduced in AM-Tg mice via suppression of vascular permeability. *In vitro*, AM exerted direct antiapoptotic and neurogenic actions on neuronal cells. Exogenous administration of AM in mice after 20m-MCAO also reduced the infarct area, and promoted vascular regeneration and functional recovery. In summary, this study suggests the neuroprotective and vasculo-neuro-regenerative roles of AM and provides basis for a new strategy to rescue ischemic brain through its multiple hormonal actions. (*Endocrinology* 147: 1642–1653, 2006)

ADRENOMEDULLIN (AM) IS a potent vasodilating peptide comprising 52 amino acids, which was originally isolated from human pheochromocytoma tissues in 1993 as a substance to elevate cAMP concentration in platelets (1). It is secreted mainly from the vascular wall into circulating blood to reduce pre- and post-load on the heart via vasodilation, natriuresis, and suppression of aldosterone release. Intravenous administration of AM to patients with heart failure or pulmonary hypertension has already been initiated and beneficial hemodynamic effects have been reported (2).

Along with its vasodilating effect, a number of studies have demonstrated various and significant effects of AM on the regulation of vascular structure, including its development, remodeling, and regeneration. Mice lacking the AM gene did not survive their embryonic stage and showed abnormal vasculature with sc hemorrhage (3, 4). Mice overexpressing AM in endothelial cells were revealed to be hypotensive and resistant to vascular remodeling such as neointima formation caused by cuff injury, and atherogenesis associated with a high-cholesterol diet (5). We have recently established that AM promotes endothelial regeneration in the wound healing assay using cultured endothelial cells and enhances neovascularization *in vivo* into sc implanted gel-plugs in mice (6, 7). We and others (8–11) have further demonstrated that the potentiating action of AM on vascular regeneration is mediated by activation of the phosphatidyl inositol-3 kinase (PI3K)-Akt pathway.

Recently, it has been known that AM is secreted from various organs including the heart, lung, kidney, adipose tissues, and central nervous system (12). Moreover, AM expression has been demonstrated to be markedly enhanced by ischemia through the activation of hypoxia-responsive elements in the AM gene via transcription factor hypoxia-inducible factor-1. In the central nervous system, where AM is

---

First Published Online December 29, 2005

Abbreviations: AM, Adrenomedullin; ANCOVA, analysis of covariance; BP, blood pressure; BrdU, bromodeoxyuridine; CGRP, calcitonin gene-related peptide; diHE, dihydroethidium; GFAP, glial fibrillary acidic protein; LDPI, laser Doppler perfusion imager; MCA, middle cerebral artery; 20m-MCAO, middle cerebral artery occlusion for 20 min; NeuN, neuronal marker; NHNP, normal human neuronal progenitor cells; PAMP, proadrenomedullin N-terminal 20 peptide; PECAM, platelet endothelial cell adhesion molecule; PI3K, phosphatidyl inositol-3 kinase; PKA, protein kinase A; ROS, reactive oxygen species; ssDNA, single-strand DNA; Tg, transgenic; Wt, wild type.

Endocrinology is published monthly by The Endocrine Society (http://www.endo-society.org), the foremost professional society serving the endocrine community.

Endocrinology, April 2006, 147(4):1642–1653

mainly expressed in neurons and the endothelium (13), it is reported that transient ischemia boosted AM expression for more than 15 d (14). However, the role of augmented AM has remained unclear for inconsistent previous results. three studies reported neuroprotective effects of AM by demonstrating reduction of infarct size after transient ischemia (15–17), whereas one study detected exacerbation of infarction as a result of AM infusion (14).

In this context, our study presented here focused on the roles of augmented AM in ischemic brain and examined its therapeutic potential. We generated new lines of transgenic mice that overproduce AM (AM-Tg) in the liver that mimics chronic AM administration. After inducing 20-min middle cerebral artery occlusion (20m-MCAO) to produce a nonfatal stroke model in the AM-Tg mice, we observed the long-term effects of AM on the ischemic brain up to postoperative d 56. We examined the mice for the recovery of blood flow in the ischemic region and impaired motor function after stroke, and immunohistochemically examined the ischemic striatum to determine effects of AM on neuronal loss/apoptosis, gliosis, leukocyte infiltration, oxidative stress, vascular regeneration, and neurogenesis after 20m-MCAO. In addition, another stroke model, 2-h middle cerebral artery occlusion (2 h-MCAO), was performed to observe the effect of AM in acute phase of the fatal stroke. *In vitro* studies using neuronal progenitor cells or rat pheochromocytoma PC12 cells were performed to examine direct antiapoptotic and neurogenic actions of AM on these neuronal cells. Finally, we investigated the effect of exogenous AM administration after 20m-MCAO to determine the appropriate amount and timing of AM treatment after cerebral ischemia.

Materials and Methods

Generation of transgenic mice which overproduce human AM but do not overproduce mature proadrenomedullin N-terminal 20 peptide (PAMP)

The AM gene contains coding regions for not only AM but also PAMP, a different vasodilating peptide. Amidation at their carboxyl terminals after their synthesis is needed for both AM and PAMP to exert their biological activity. The bioactive amidated forms are known as mature AM and mature PAMP, respectively. To identify the specific effects of AM, we generated a transgene construct with a point mutation on the PAMP amidation signal in the full-length AM gene cDNA. Guanine was substituted for cytosine on the 3' end of the PAMP coding region so that glycine on the C' terminal of the PAMP product was replaced with alanine. In this way, amidation and maturation of PAMP by peptidylglycine α-hydroxylase and α-hydroxyglycine N-C lyase were inhibited (Fig. 1A). The mutant AM gene cDNA was then inserted into a plasmid containing the human serum amyloid P component promoter, which is widely used to target gene expression specific to the liver. When the product is secreted from the liver, it mimics intravenous administration of the agent. The *Hin*dIII-*Xho*I fragment of the plasmid was microinjected into the pronucleus of fertilized C57BL/6J mice eggs.

The copy number of transgenes was quantified by means of genomic Southern blotting according to standard procedure. Plasma concentrations of human total AM and mature AM were measured with a commercially available immunoradiometric assay (Cosmic, Tokyo, Japan).

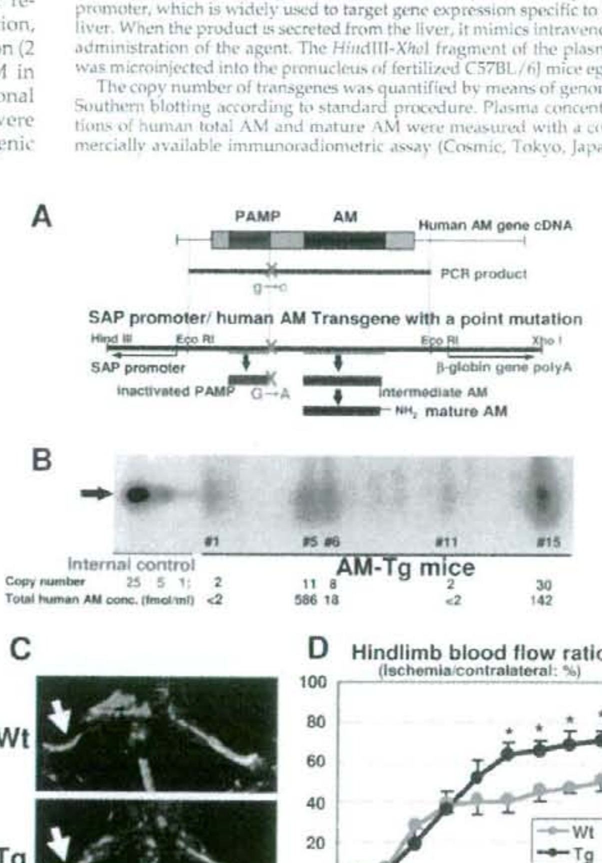

FIG. 1. Generation of transgenic mice which overproduce AM but do not overproduce mature PAMP in the liver and augmented angiogenesis in the transgenic mice after femoral artery occlusion. A, Schematic representation of the transgene construct derived from human AM gene cDNA with a point mutation in the amidation signal of PAMP. B, Southern blot analysis of the tail DNA of the founder mice. *Arrow*, Blots for the transgene. Internal controls for indicated copies are located in the *left three lanes*. The line No. indicates the mice in which the transgene was detected by PCR. The copy numbers estimated by densitometry and the plasma concentrations of total human AM in F3 mice of the lines are shown. C, Hindlimb blood flow analyzed by LDPI. *Red* or *white* indicates a higher flow than *blue* or *green*. *Arrows*, Comparison of ischemic hindlimbs between Wt and AM-Tg on d 28 after femoral artery ligation. D, Quantitative analysis of the hindlimb blood flow in ischemia. *, $P < 0.05$ for Wt *vs.* AM-Tg by ANCOVA; n = 6.

Human mature PAMP concentration was measured with a recently developed enzyme immunoassay (18). To determine the brain concentration of AM, we used the RIA kits for measurement of human and mouse total AM (Phoenix, Belmont, CA), according to the manufacturer's instruction. Blood pressure (BP) was measured with tail cuff (Softron, Tokyo, Japan). Hindlimb ischemia was induced by ligating the right femoral artery and blood flow of the ischemic limb was estimated with a laser Doppler perfusion imager (LDPI; Moor Instruments Ltd., Devon, UK) to confirm the angiogenic effect of AM-Tg mice. The perfusion ratio (%) was calculated as that of the ipsilatereal to the contralateral side. Animal care and experiments were in accordance with the guidelines for animal experiments of Kyoto University.

Induction of stroke by MCAO

We performed nonfatal 20m-MCAO and fatal 2 h-MCAO by the standard *trans*-luminal method, which has been described in various previous reports (19). Briefly, a 8–0 nylon monofilament coated with silicone was inserted from the left common carotid artery via the internal carotid to the base of the left middle cerebral artery (MCA) of 12-wk-old mice anesthetized with 5% halothane and maintained on 1%. After 20 min or 2 h of occlusion, the filament was withdrawn; and the arteries were reperfused, whereas the left common carotid artery was permanently ligated. Occlusion and reperfusion of the MCA was confirmed by means of fiber-shaped laser Doppler perfusion imager (Omegawave, Tokyo, Japan). We observed the mice until postoperative d 56 to examine blood flow in the ischemic region with an LDPI and motor function with a rota-rod exercise test.

Immunohistochemical examination of the ischemic striatum

After the induction of 20m-MCAO, mice were killed on postoperative d 0–56 and the harvested brains were subjected to immunohistochemical examination using a standard procedure described elsewhere (20). We used these primary antibodies: neuronal marker, NeuN (1:200; Chemi-Con, Temecula, CA); astrocyte marker, glial fibrillary acidic protein (GFAP) (1:400; Chemicon); apoptosis marker, single-strand DNA (ssDNA) (1:50; Dako, Carpinteria, CA); leukocyte marker, CD45 (1:100, PharMingen, San Diego, CA); endothelial marker, platelet endothelial cell adhesion molecule (PECAM)-1 (CD31) (1:100, PharMingen); and a marker for proliferating cells, bromodeoxyuridine (BrdU) (1:50, Molecular Probes, Eugene, OR); to examine infarct area, gliosis, leukocyte infiltration, apoptosis, vascular regeneration and neurogenesis. Briefly, free-floating 30-μm coronal sections at the level of the anterior commissure were stained and observed with a confocal microscope (LSM5 PASCAL; Carl Zeiss SMT AG, Oberkochen, Germany). The infarct area (mm^2/field) was defined and quantified as the region where loss of NeuN immunoreactivity was observed and gliosis (mm^2/field) as the area stained GFAP in the ischemic striatum at $\times$ 5 fields. CD45 or ssDNA-positive cells (cells/mm^2) were quantified to serve as an index of leukocyte infiltration or of apoptosis, respectively, in the ischemic core at $\times$20 magnification. Capillary density was quantified as the number of PECAM-1-positive cells (cells/mm^2). The vessel counts were performed in the region of ischemic core at 0.5–1.0 mm anterior from the bregma. We prepared two thin sections (6 μm thickness) per mouse for vessel counting and four representative fields from each section were evaluated for capillary density in the ischemic core. To examine neurogenesis, mice were injected ip with BrdU 50 mg/kg (Sigma-Aldrich Co., St. Louis, MO) twice daily on postoperative d 4–6 and the number of BrdU-NeuN double-positive cells (cells/mm^2), which are generally defined as regenerated neurons, were quantified to serve as an index of neurogenesis. We also examined the production of reactive oxygen species (ROS) *in situ* by using the oxidative fluorescent dye dihydroethidium (diHE; 2×10^{-6} M; Sigma).

Quantification of $CD34^+$ mononuclear cells after 20m-MCAO

We counted peripheral $CD34^+$ mononuclear cells according to the International Society of Hematotherapy and Graft Engineering (ISHAGE) guidelines (21). Briefly, peripheral blood was taken from the orbital vein and stained with CD34-PE and CD45-FITC monoclonal antibodies (BD PharMingen, San Jose, CA) in a TruCOUNT tube (BD PharMingen) according to the manufacturer's instruction. After the reaction, $CD34^+$-$CD45^{dim}$ cells were quantified as $CD34^+$ mononuclear cells by a fluorescence-activated cell sorting machine Aria (BD) by using the ISHAGE sequential gating strategy (21).

Analysis of infarct volume and brain edema after 2 h-MCAO

We performed 2 h-MCAO to examine the effect of AM in the acute phase of fatal stroke. To estimate infarct or edema volume, mice were killed 24 h after the occlusion. The brain was removed and cut into 2 mm-thick slices and immersed in saline containing 2% 2,3,5-triphenyltetrazolium chloride for 30 min at 4 C. Infarct or edema volume was calculated as the percentage volume of the contralateral hemisphere with a standard procedure as described elsewhere (22). We estimated Evans Blue leakage in the brain parenchyma as previously reported (23), to serve as an index of vascular permeability *in situ*. Briefly, 0.2 ml of 2.5% Evans Blue solution was injected into mice via a tail vein 10 min before 2 h-MCAO and mice were killed at 24 h after the ischemia. Brain tissues were weighed and homogenized in 50% trichloroacetic acid solution to extract the dye in the supernatant. The tissue content of Evans Blue was estimated from the absorbance of 620 nM.

Estimation of apoptosis and differentiation of neuronal cells

The ratio of apoptotic cells was examined using normal human neuronal progenitor cells (NHNP; Cambrex Bioscience, Walkersville, MD). Cells were plated at a density of 5×10^4 cells/cm^2 on a laminin-coated 24-well dish and incubated in serum-free neuronal basal medium for 48 h. After the experimental period, the cell number was assessed by 5-mercapto-1-methyltetrazole assay (Nakalai Tesque), and the cells were stained with an anti-ssDNA antibody and nuclear staining propidium iodide to calculate the ratio of apoptotic cells to the total cells in each microscopic image.

Neuronal differentiation was examined as described previously (24), using rat pheochromocytoma PC12 cells (Riken Gene Bank, Tsukuba, Japan). Briefly, the length of the neuronal process (micrometers/cell) was calculated to serve as an index of neuronal differentiation after plating at a density of 10^4 cells/cm^2 on a collagen I-coated 24-well dish and incubated in 1% serum DMEM for 7 d. The cells were treated with 10^{-5}mol/liter AM or 100 ng/ml nerve growth factor as a positive control, and with the following inhibitors: the two AM antagonists, 10^{-5}mol/liter AM (22–52) and 10^{-5} mol/liter calcitonin gene-related peptide(8–37) [CGRP(8–37)] (Peptide Institute Inc., Osaka, Japan), the two protein kinase A (PKA) inhibitors, 10^{-5} mol/liter adenosine 3P,5P-cyclic monophosphorothioate Rp-isomer (Rp-cAMP) and 10^{-6} mol/liter myristoylated cell-permeable PKA inhibitor peptide sequence (14–22) (PKA Inh), and the two PI3K inhibitors, 10^{-5} mol/liter LY294002 and 10^{-7} mol/liter wortmannin (Calbiochem, San Diego, CA). For endothelial cell coculture experiments, human umbilical vein endothelial cells (HUVEC; Cambrex) were plated into transwell membrane inserts at a density of 10^5 cells/cm^2.

Exogenous administration of AM and hydralazine

Recombinant human mature AM dissolved in 0.9% saline was exogenously administrated to C57BL/6J wild-type mice (Wt) by means of osmotic pumps (Alzet Model 2002; Alzet Osmotic Pumps Co., Cupertino, CA) at a rate of 50 ng/h, which is estimated to achieve a plasma concentration of 2 fmol/ml (25). To determine appropriate timing to start AM treatment after 20m-MCAO, we implanted the pump ip just after the operation (d 0), or at 24 (d 1) or 72 h (d 3) later. We killed the mice on d 7 for histological examination and the period of the exogenous AM treatment was from d 0, 1, or 3 to d 7. In some experiments, low-dose (0.1 mM) hydralazine was exogenously administrated in drinking water.

Statistics

All data were expressed as mean ± SE. Comparison of means between two groups was performed with Student's *t* test. When more than two groups were compared, ANOVA was used to evaluate significant differences among groups, and if significant differences were confirmed, each difference was further examined by means of multiple comparisons. We

TABLE 1. Plasma concentrations of human AM and systolic BP in Wt and three lines of AM-Tg mice

	Wt	Low conc.	Medium conc.	High conc.
Total AM (fmol/ml)	1.1 ± 0.2	17.6 ± 4.4[a]	142.2 ± 18.4[a]	585.5 ± 117.7[a]
Mature AM (fmol/ml)	0.5 ± 0.4	2.6 ± 0.6[a]	10.4 ± 2.4[a]	24.9 ± 4.2[a]
Systolic BP (mm Hg)	122.7 ± 1.6	113.0 ± 2.5[a]	113.4 ± 2.6[a]	109.4 ± 2.5[a]

conc., Concentration.
[a] $P < 0.01$ vs. Wt; n = 4–12.

performed analysis of covariance (ANCOVA) when repeated-measurement had done, specifically, in the rota-rod test and laser Doppler flowmetry. Probability was considered to be statistically significant at $P < 0.05$.

Results

Generation of transgenic mice that overproduce human AM but do not overproduce mature PAMP

We generated seven lines of founder mice carrying the transgene and maintained three of them (lines 5, 6, and 15). Their plasma concentrations of human total AM were 585.5 ± 117.7, 17.6 ± 4.4 and 142.2 ± 18.4 fmol/ml and the copy numbers of the transgene estimated by Southern blot densitometry analysis were 11, 8, and 30, respectively (Fig. 1B). The physiological concentration of mouse total AM is reportedly 5–10 fmol/ml, so that the transgenic mice were expected to overproduce AM about 100, 3, and 30 times more than endogenous AM. The three lines were designated low (no. 6), medium (no. 15), and high (no. 5) concentration line according to their plasma AM concentration. The high concentration line (no. 5) was used for further study unless otherwise indicated. The plasma concentration of human mature AM, the bioactive amidated form, increased to 2.6–24.9 fmol/ml in the AM-Tg mice (Table 1). On the other hand, plasma human mature PAMP did not change in AM-Tg mice. The concentration (fmol/ml) was 2.21 ± 0.58 in Wt *vs.* 2.15 ± 0.35 in AM-Tg (n = 6), so that the point mutation on the amidation signal in the PAMP coding region was expected to successfully inhibit maturation of PAMP. There were no apparent differences in overall appearance, behavior, growth or fertility between Wt and AM-Tg mice. The systolic BP in 12-wk-old mice was significantly reduced in all three lines of AM-Tg compared with Wt. The BP (mm Hg) was 122.7 ± 1.6 in Wt *vs.* 109.4 ± 2.5–113.4 ± 2.6 in AM-Tg, depending on the line ($P < 0.05$; n = 5; Table 1).

Therapeutic angiogenesis in hindlimb ischemia model was promoted in AM-Tg mice

The recovery of blood flow in the ischemic hindlimb of Wt and AM-Tg mice was compared and was found to have

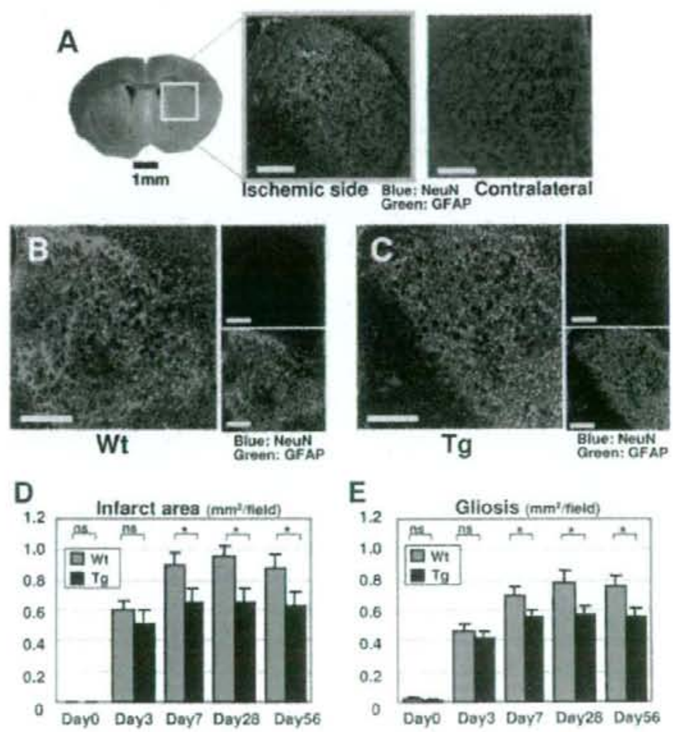

FIG. 2. Effects of AM on infarct area and gliosis after the nonfatal stroke, 20m-MCAO. A, Histological examination of the ischemic striatum. The outlined field was examined for infarct area and gliosis. The ischemic side and contralateral side on d 3 after 20m-MCAO are shown. *Scale bar*, 500 μm (×5 magnification). B and C, Representative images of the ischemic striatum on postoperative d 7 stained for NeuN (*blue*) and GFAP (*green*). Infarct area, defined as the region where NeuN immunoreactivity was lost, and gliosis, defined as the area where GFAP immunoreactivity was observed, in Wt (B) and AM-Tg (C) are shown. *Scale bar*, 500 μm (×5 magnification). D and E, Quantitative analysis of the infarct area (D) and gliosis (E). *, $P < 0.05$; ns, not significant for Wt *vs.* AM-Tg; n = 12.

significantly improved in AM-Tg mice after postoperative d 17. The hindlimb blood flow ratio on d 28 (ipsilateral/contralateral, %) was 56.6 ± 8.3 in Wt *vs.* 73.8 ± 5.3 in AM-Tg ($P < 0.05$; n = 6; Fig. 1, C and D). In this way, promotion of therapeutic angiogenesis by AM was confirmed in AM-Tg mice.

Brain remodeling in ischemic striatum after 20m-MCAO

We investigated the time course of neuronal loss, reactive gliosis, vascular regeneration, and neuronal regeneration; the entire process can be defined as "brain remodeling" after ischemia.

20m-MCAO caused selective loss of NeuN-positive cells and marked reactive gliosis (Fig. 2A) in the ipsilateral striatum within 24 h after the operation; this condition was different from pan-necrosis caused by longer MCAO (*e.g.* 2 h-MCAO). The infarct area, that is, the area of neuronal loss, expanded progressively up to d 7, and then showed gradual increase in size until d 56, whereas gliosis spread in parallel. The expansion of the infarct area in the subacute to chronic phase after mild stroke was compatible with previously reported findings (26). Vascular regeneration in the striatum with enhanced capillary density was obvious after postoperative d 7, and subsequent neurogenesis became obvious after d 28.

The concentrations of the overproduced human AM (fmol/g tissue) in the ischemic brain of AM-Tg mice before and on postoperative d 1 and 28 after 20m-MCAO were 27.8 ± 10.3, 87.4 ± 4.0 and 30.3 ± 16.8, respectively. Those of endogenous mouse AM (fmol/g tissue) were 3.7 ± 2.1, 7.2 ± 2.5, and 4.6 ± 3.0.

Infarct area and gliosis were reduced in AM-Tg mice after 20m-MCAO along with suppression of leukocyte infiltration and ROS production

A significant decrease in infarct area and gliosis was observed in AM-Tg mice (Fig. 2, B–E) after postoperative d 7, but was not obvious on d 3. The infarct area (mm^2/field) on d 56 was 0.88 ± 0.08 in Wt *vs.* 0.64 ± 0.08 in AM-Tg ($P < 0.05$; n = 12; Fig. 2D), and gliosis (mm^2/field) on the same day was 0.76 ± 0.08 in Wt and 0.56 ± 0.07 in AM-Tg ($P < 0.05$; n = 12; Fig. 2E). Leukocyte infiltration quantified as the number of $CD45^+$ cells was significantly suppressed in AM-Tg mice especially from d 3–7. $CD45^+$ cells on d 3 ($/mm^2$) numbered 197.5 ± 16.6 in Wt *vs.* 140.7 ± 14.6 in AM-Tg ($P < 0.05$; n = 12; Fig. 3, A, B, and G). *In situ* ROS production detected by immunostaining for diHE, which stained the nucleus of $NeuN^+$ or $GFAP^+$ cells, was enhanced in Wt compared with that in AM-Tg mice (Fig. 3, C and D). Apoptotic cells quantified as the number of $ssDNA^+$ cells in the ischemic core were significantly reduced in the AM-Tg mice on d 3–7. $ssDNA^+$ cells ($/mm^2$) on d 3 numbered 214.8 ± 19.6 in Wt *vs.* 123.2 ± 11.1 in AM-Tg ($P < 0.01$; n = 12; Fig. 3, E, F, and H).

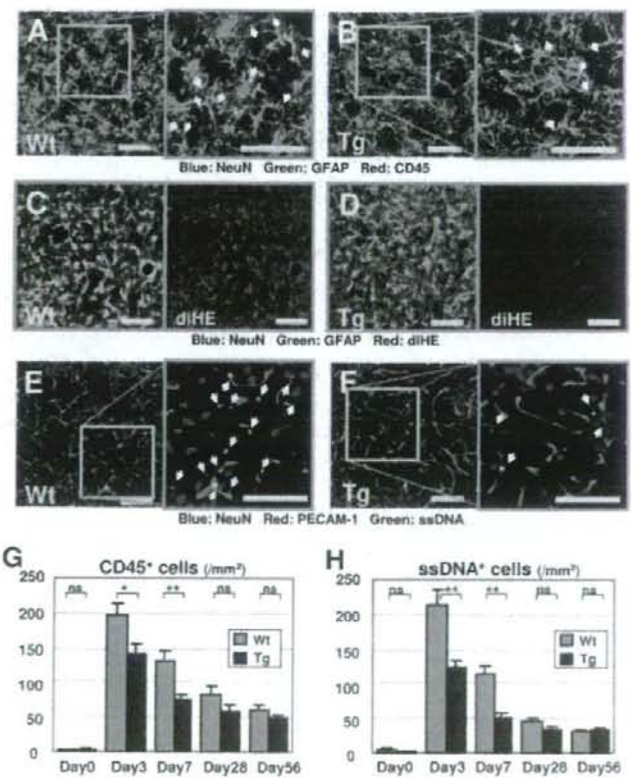

FIG. 3. Effects of AM on leukocyte infiltration, ROS production, and apoptosis in the ischemic brain after 20m-MCAO. A and B, Detection of leukocyte infiltration in the ischemic core on postoperative d 7 by immunostaining for $CD45^+$ cells (*red*) in Wt (A) and AM-Tg (B). *Arrows*, $CD45^+$ cells. C and D, *In situ* detection of ROS in ischemic striatum on postoperative d 7 by immunostaining for diHE (*red*) in Wt (C) and AM-Tg (D). E and F, Detection of apoptotic cells in the ischemic core on postoperative d 7 by immunostaining for $ssDNA^+$ cells (*green*) in Wt (E) and AM-Tg (F). *Arrows*, $ssDNA^+$ cells. G and H, Quantitative analysis of $CD45^+$ cells (G) and $ssDNA^+$ cells (H) in the ischemic core. *, $P < 0.05$; **, $P < 0.01$; ns, not significant for Wt *vs.* AM-Tg; n = 12. *Scale bar*, 100 μm (×20 magnification).

Vascular regeneration was augmented in AM-Tg mice after 20m-MCAO associated with increased mobilization of CD34⁻ mononuclear cells

The blood flow in the ischemic brain estimated by LDPI was significantly higher in AM-Tg mice after postoperative d 7 and higher flow was maintained until d 56. The brain blood flow ratio (ipsilateral/contralateral, %) on d 56 was 88.9 ± 2.8 in Wt *vs.* 97.6 ± 3.0 in AM-Tg ($P < 0.01$ by ANCOVA; n = 8; Fig. 4, C, D, and H). We were also able to confirm that capillary density determined as the number of PECAM-1⁺ cells was augmented in AM-Tg mice. The density (/mm^2) on d 56 was 468.8 ± 21.8 in Wt *vs.* 536.6 ± 13.6 in AM-Tg ($P < 0.05$; n = 8; Fig. 4I). Thus, the physiological neovascularization in the ischemic core after stroke was augmented in AM-Tg mice. Peripheral CD34⁻ mononuclear cells were physiologically enhanced after 20m-MCAO and further increased in AM-Tg mice on d 3–7. The cells (/ml) on d 3 numbered 1774 ± 272 in Wt *vs.* 3199 ± 562 in AM-Tg ($P < 0.05$; n = 6; Fig. 5, A–C).

Augmented neurogenesis and improved recovery of impaired neurological function were observed in AM-Tg mice after 20m-MCAO

BrdU injection on postoperative d 4–6 proved that most BrdU-positive cells were costained with GFAP (data not shown) and that there were far fewer BrdU-PECAM-1 or BrdU-NeuN double-positive cells. We found that regenerated neurons defined as BrdU-NeuN double-positive cells were frequently detected adjacent to the vasculature and the number of these cells on d 56 was correlated with capillary density ($P = 0.003$; n = 12; Fig. 6, A and B; and Table 2). The cells increased from postoperative d 7–56, and their number was significantly higher in AM-Tg mice. The regenerated neurons (/mm^2) on d 56 numbered 20.4 ± 3.9 in Wt *vs.* 33.9 ± 4.7 in AM-Tg ($P < 0.05$; n = 12; Fig. 6C).

Recovery of impaired motor function after 20m-MCAO, quantified as the exercise time on an accelerating rota-rod from the start to collapse down, was significantly better in AM-Tg mice. The exercise time (second) on d 49 was 21.5 ± 1.5 for Wt *vs.* 27.1 ± 2.0 for AM-Tg ($P < 0.01$ by ANCOVA; n = 14; Fig. 6D). To confirm whether vasculogenesis and neurogenesis are the contributing factor to the recovery from the ischemic damage, we analyzed the relation between capillary density, the number of regenerated neuron and the rota-rod result in AM-Tg mice after 20m-MCAO. As shown in Table 2, we found that the capillary density was significantly correlated with the rota-rod exercise time ($P = 0.005$; n = 24) and neurogenesis tended to be correlated with it ($P = 0.08$; n = 12).

Low-concentration AM-Tg mice also showed reduced infarct area and promoted vascular regeneration

We performed 20m-MCAO, using the low-concentration AM-Tg mice (plasma mature AM, 2.6 ± 0.6 fmol/ml) as well as the high-concentration line (plasma mature AM, 24.9 ± 4.2 fmol/ml) to determine appropriate concentration for AM

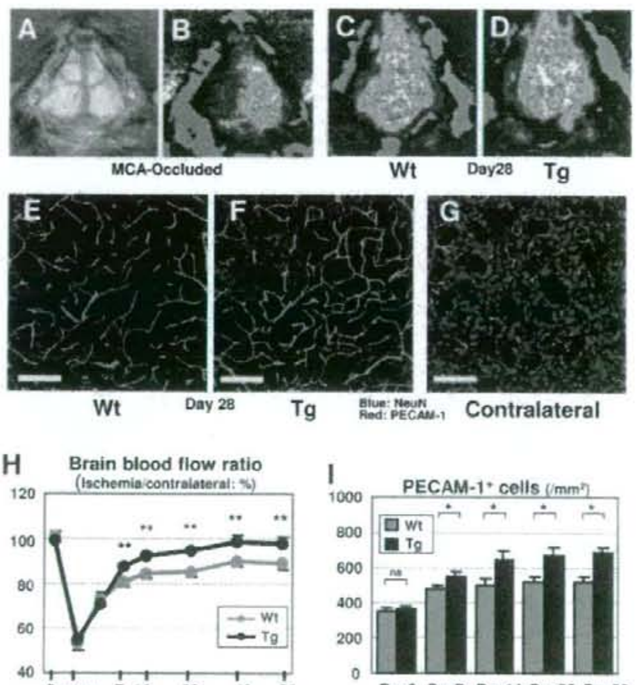

FIG. 4. Effects of AM on vascular regeneration in the ischemic brain after 20m-MCAO. A–D, Analysis of the blood flow in the ischemic brain by LDPI evaluated in mice with the scalp removed (A). Flowmetric analysis of the ischemic brain during MCA-Occlusion (B) and on d 28 after 20m-MCAO in Wt (C) and AM-Tg (D). *Red* or *white* indicates higher flow than *blue* or *green*. E–G, Histological examination of the vasculature in the ischemic core with PECAM-1 staining. Ischemic striatum on d 28 after 20m-MCAO in Wt (E) and AM-Tg (F), and contralateral nonischemic striatum (G). *Scale bar*, 100 μm (×20 magnification). H, Quantitative analysis of the blood flow in the ischemic brain. Comparison of recovery from ischemia after 20m-MCAO between Wt and AM-Tg. MCA-Oc, blood flow during MCA occlusion; **, $P < 0.01$ for Wt *vs.* AM-Tg by ANCOVA; n = 8. I, Quantitative analysis of capillary density in the ischemic brain. Comparison of time course for increase in capillary density, determined as the number of PECAM-1⁺ cells, between Wt and AM-Tg mice. *, $P < 0.05$; ns, not significant; n = 8.

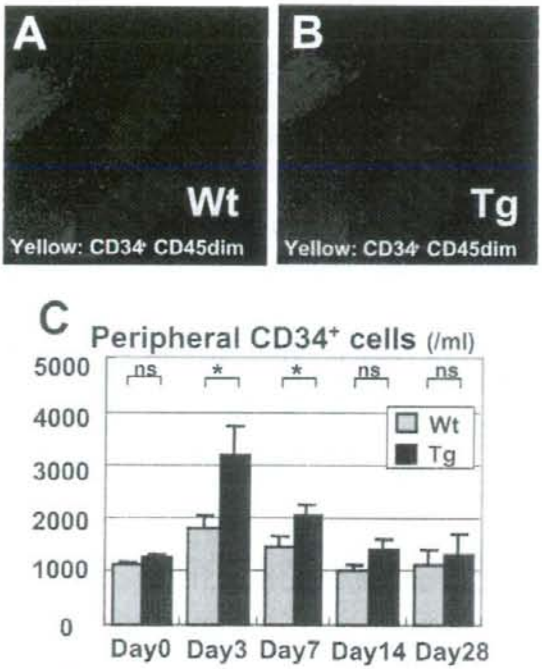

FIG. 5. Effects of AM on mobilization of CD34+ mononuclear cells into peripheral blood after 20m-MCAO. A–C, Quantification of CD34+ mononuclear cells after 20m-MCAO. Scatter plots for fluorescence-activated cell sorting analysis of the CD34+ cells in peripheral blood of Wt (A) and AM-Tg (B) on postoperative d 3. *Yellow*, CD34+-CD45dim mononuclear cells. Comparison of the time course for mobilization of CD34+ cells into peripheral blood between Wt and AM-Tg (C). *, $P < 0.05$; ns, not significant; n = 6.

treatment. The result showed comparable levels of neuroprotection and vascular regeneration between the low-concentration line and the high-concentration line (Table 3). We further analyzed BP-matched mice by administration of low-dose hydralazine (0.1 mM in drinking water) to exclude the possibility that lower BP observed in AM-Tg mice caused beneficial effects after 20m-MCAO. As shown in Table 3, lower BP alone did not reduce the infarct area nor promote vascular regeneration, although hydralazine administration caused BP reduction comparable to that in AM-Tg mice.

Brain edema was reduced in AM-Tg mice at 24 h after 2 h MCAO

The survival rate of mice after the fatal stroke, 2 h-MCAO, was 0% on d 7. We observed no significant difference in the rate between Wt and AM-Tg mice. The edema volume was reduced in AM-Tg mice 24 h after 2 h-MCAO; although the infarct volume showed no significant difference between them. Edema volume (% volume of contralateral hemisphere) was 13.5 ± 1.2 in Wt *vs.* 9.7 ± 0.9 in AM-Tg ($P < 0.05$; n = 9, Fig. 7C), whereas infarct volume (% volume of contralateral hemisphere) was 39.0 ± 4.9 in Wt *vs.* 44.5 ± 7.3 in AM-Tg (not significant; n = 9; Fig. 7, A and B). As shown in Fig. 7D, we found that Evans Blue leakage into the ischemic

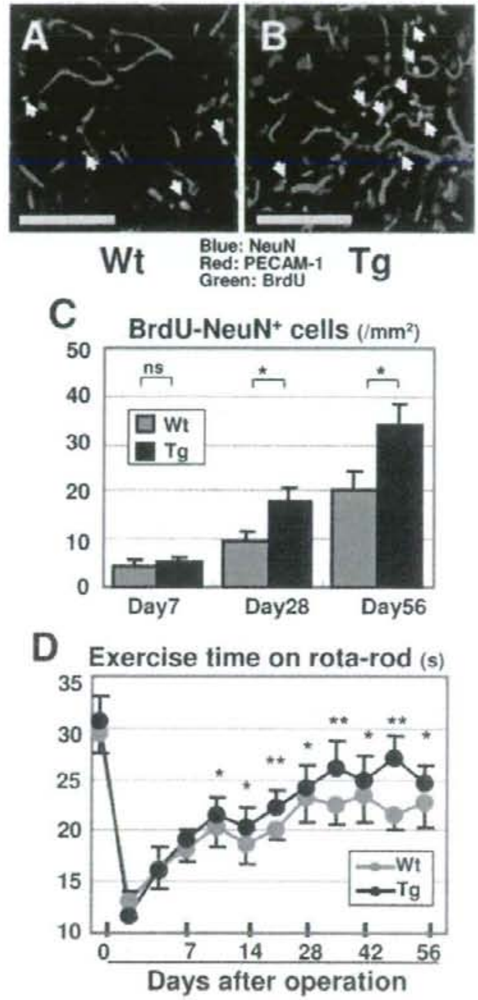

FIG. 6. Effects of AM on neurogenesis and recovery of impaired motor function after 20m-MCAO. A and B, Detection of regenerated neurons on postoperative d 56 by immunostaining for BrdU and NeuN. *Arrows*, BrdU-NeuN double-positive cells in the ischemic core of Wt (A) and AM-Tg (B). *Scale bar*, 100 μm. C, Quantitative analysis of regenerated neurons. *, $P < 0.05$; ns, not significant; n = 12. D, Recovery of impaired motor function after 20m-MCAO, quantified as the exercise time on an accelerating rota-rod from the start to collapse down. *, $P < 0.05$; **, $P < 0.01$ for Wt *vs.* AM-Tg by ANCOVA; n = 14.

core was significantly reduced in AM-Tg mice. The content of Evans Blue (ng/g tissue) in the ischemic brain at 24 h after 2 h-MCAO was 239.4 ± 37.3 in Wt *vs.* 133.9 ± 9.4 in AM-Tg ($P < 0.01$; n = 4; Fig. 7E).

AM exerted direct antiapoptotic and neurodifferentiating effects on neuronal cells in vitro

After 48 h incubation of NHNP under serum-free apoptotic conditions, in which the number of the cells had decreased

TABLE 2. Significant correlation between the regenerative elements and apoptosis, neurogenesis, and functional recovery after 20m-MCAO

X	Y	Regression line	*P*
Capillary density (% field)	Apoptotic cells (/mm^2)	Y = −2.3X−37	0.01
Capillary density (% field)	Regenerated neuron (/mm^2)	Y = 3.2X-21	0.003
Capillary density (% field)	Rota-rod result (sec)	Y = 1.3X+9	0.005
Regenerated neuron (/mm^2)	Rota-rod result (sec)	Y = 0.3X+19	0.08

n = 12–24.

to half, the viable cell number was increased in the AM 10^{-8} mol/liter-treated group to 38.8 ± 7.1% over the control ($P < 0.01$; n = 4; Fig. 8C). The ratio of ssDNA$^+$ cells to total cells (%) was 9.8 ± 1.9 in Wt *vs.* 4.0 ± 0.6 in the AM 10^{-8} mol/liter-treated group ($P < 0.05$; n = 4; Fig. 8, A, B, and D).

After 7-d incubation of PC12 cells under differentiation condition, both the cell number and the length of neuronal process increased dose dependently as a result of AM treatment ($P < 0.01$; n = 6; Fig. 8, E and I). Coculture with endothelial cells also increased the cell number and the length of neuronal process. The effect of AM was canceled by AM blockers, PKA inhibitors, and PI3K inhibitors (Table 4).

Exogenous administration of AM reduced infarct area, promoted vascular regeneration, and improved neurological function after 20m-MCAO

We further examined the effects of exogenous infusion of mature AM by means of an osmotic pump in the amount reported to achieve a plasma concentration of 2 fmol/ml. Implantation of the pump just after the operation resulted in increase in the blood flow and reduction of the infarct area on postoperative d 7 to a comparable level to those in AM-Tg mice. Moreover, the treatment started at 24 h after the operation (d 1) showed almost the same therapeutic effect. However, the implantation at 72 h after the operation (d 3) failed to reveal any significant effect (Fig. 9, A and B). The rota-rod exercise time was significantly improved in the AM-treated group. The exercise time (second) on d 7 was 17.0 ± 1.5 in vehicle group *vs.* 18.1 ± 2.0 in AM-treated group (n = 6 for vehicle group and 12 for AM-treated group; $P < 0.05$ by ANCOVA).

Discussion

In the present study, we generated novel transgenic mice that overproduce AM in their liver without overproduction of mature PAMP and investigated the roles of AM in degeneration or regeneration processes after brain ischemia, which can be defined as brain remodeling, as summarized in Fig. 10. Brain edema in acute phase, neuronal loss and gliosis in subacute to chronic phase after 20m-MCAO were reduced in AM-Tg mice. Furthermore, vascular regeneration, mobilization of CD34$^+$ mononuclear cells and subsequent neurogenesis were enhanced in them. These effects resulted in improved recovery of motor function after the nonfatal stroke. AM was also found to exert direct antiapoptotic and neuro-differentiating effects on neuronal cells *in vitro*. Exogenous administration of AM in mice after 20m-MCAO also

TABLE 3. Comparison of the effects on neuroprotection and vascular regeneration after 20m-MCAO between Wt control mice, hydralazine-administrated mice, and the low and high concentration lines of AM-Tg

Mice	Infarct area (mm^2/field)	Brain blood flow (% Contralateral)	Systolic BP (mm Hg)
Control	0.90 ± 0.09	80.8 ± 2.3	120.1 ± 2.2
Hydralazine	0.94 ± 0.17^{ns}	79.6 ± 2.6^{ns}	101.0 ± 3.9^a
Low-conc. AM-Tg	0.58 ± 0.12^b	88.4 ± 2.9^b	105.1 ± 1.8^a
High-conc. AM-Tg	0.67 ± 0.09^b	86.3 ± 2.0^b	106.4 ± 3.5^a

conc., Concentration.
^{a} $P < 0.01$; ^{b} $P < 0.05$; ns, not significant *vs.* control; n = 6.

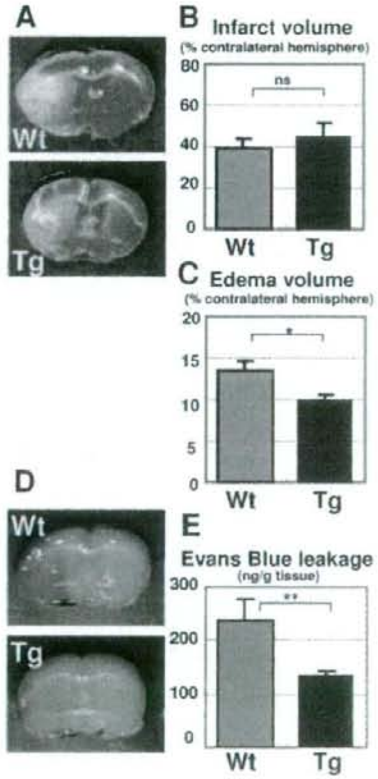

FIG. 7. Effects of AM on infarct size and brain edema in the fatal stroke, 2 h-MCAO. A, Comparison of infarct size between Wt and AM-Tg with 2,3,5-triphenyltetrazolium chloride staining at 4.0 mm from the frontal pole. *White area* represents infarction. B and C, Infarct (B) and edema (C) volumes quantified 24 h after the operation of 2 h-MCAO. *, $P < 0.05$; ns, not significant for Wt and AM-Tg; n = 9. D: Representative image of *in situ* Evans Blue leakage into the ischemic core at 24 h after 2 h-MCAO. E, Quantification of Evans Blue in the ischemic brain. **, $P < 0.01$; n = 4.

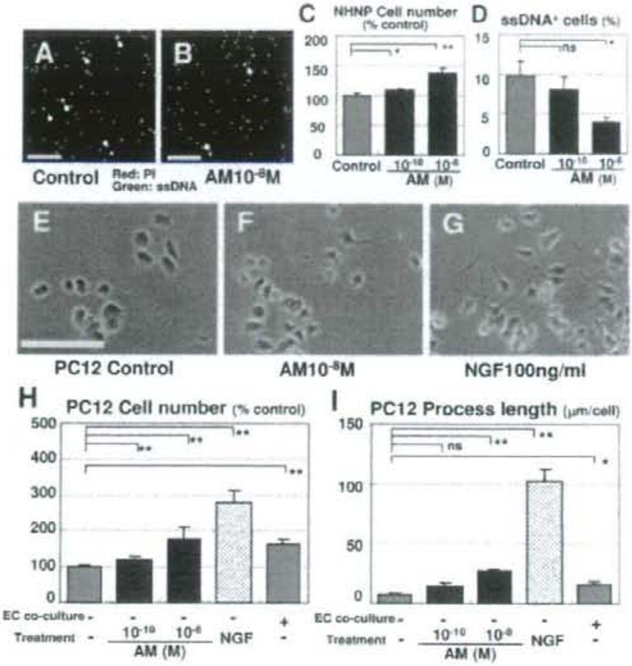

FIG. 8. Effects of AM *in vitro* on apoptosis of NHNP neuronal progenitor cells and neuronal differentiation of PC12 cells. A–D, *In vitro* analysis of apoptotic NHNP after incubation with (B) or without (A) AM. NHNP cell number (C) and the ratio of ssDNA$^+$ cells to total cells (D) after 48 h incubation. *, $P < 0.05$; **, $P < 0.01$; ns, not significant *vs.* control; n = 4; *scale bar*, 100 μm. E–G, Effects of AM on neuronal differentiation of PC12 cells evaluated by the length of neuronal process. Microscopic examination of PC12 cells after incubation for 7 d (E). AM (F) or nerve growth factor (G) was added to the culture medium. Quantification of cell number (H) and the length of neuronal process (I). *, $P < 0.05$; **, $P < 0.01$; ns, not significant; n = 6; *scale bar*, 100 μm.

reduced the infarct area, and promoted vascular regeneration and functional recovery.

Stroke causes two different types of neuronal death: necrosis and apoptosis. Acute neuronal loss, which is completed within a few days after ischemic damage, is necrotic, whereas delayed neuronal loss, which may start several days after transient ischemia, is considered to be apoptotic (27, 28). Many studies have found that treatments that reduce inflammation or oxidative stress are beneficial for the prevention of apoptotic neuronal loss (29, 30).

In this study, we demonstrated that AM exerts neuroprotective actions in the ischemic brain. A significant reduction in neuronal loss in AM-Tg mice after 20m-MCAO became obvious after postoperative d 7, but was not obvious before d 3. A significant decrease in ssDNA-positive cells inside and on the border of the ischemic area was observed in AM-Tg mice in association with a reduction in CD45$^+$ cells and *in situ* ROS production in the subacute phase. AM is therefore assumed to reduce delayed neuronal loss through suppression of the apoptotic process. Furthermore, we confirmed that AM directly suppresses apoptosis of neuronal progenitor cells *in vitro*. These findings suggest that AM exerts neuroprotective effects on the ischemic brain by reducing apoptotic neuronal loss through both its direct antiapoptotic action on neurons and indirect effect via antiinflammation and anti-ROS production. Consistent with the findings in this study, several recent reports have provided evidences for the organ-protective effects of AM against inflammation and oxidative stress (31–33). In addition, we found significant negative correlation between capillary density and apoptotic cells in the same section on postoperative d 7 after 20m-MCAO. Moreover, the infarct area kept expanding between d 7–28 in Wt mice, whereas AM-Tg mice did not show the increase in size in this period. These findings suggest that the increased blood flow in AM-Tg mice was one of the causes of neuroprotection after 20m-MCAO, although we suppose that multiple actions of AM, as described above, could also contribute for neuroprotection.

Increased vascularity is reported to be associated with improved neurological recovery in human patients with stroke (34). This implies that physiological vascular regeneration in the ischemic brain constitutes a beneficial response for the recovery of impaired neurological function. Moreover, neurogenesis after stroke even in adulthood has been demonstrated to occur in a place surrounded by the vascu-

TABLE 4. Effects of AM-antagonists, PKA inhibitors, and PI3K inhibitors on AM-induced neural differentiation of PC12 cells

	Process length (μm/cell)
PC12	6.8 ± 1.7
+AM (10^{-8} mol/liter)	23.6 ± 4.0^a
+AM+AM(22–52) (10^{-6} mol/liter)	11.8 ± 3.4^b
+AM+CGRP(8–37) (10^{-5} mol/liter)	14.8 ± 1.9^c
+AM+Rp-cAMP (10^{-5} mol/liter)	10.2 ± 2.7^c
+AM+PKA Inh (10^{-6} mol/liter)	7.2 ± 2.3^b
+AM+LY294002 (10^{-5} mol/liter)	4.6 ± 1.6^b
+AM+wortmannin (10^{-7} mol/liter)	5.4 ± 1.1^b
PC12-EC coculture	20.7 ± 2.1^a

EC, Endothelial cell.

^{a} $P < 0.01$ *vs.* PC12 without AM; ^{b} $P < 0.01$ *vs.* PC12 with AM (10^{-8} mol/liter); ^{c} $P < 0.05$; n = 8.

Endocrinology, April 2006, 147(4):1642–1653

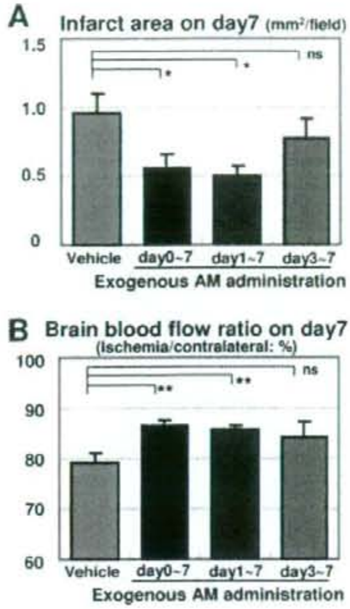

FIG. 9. Effects of exogenously administrated AM on neuroprotection and vascular regeneration after 20m-MCAO. 50 ng/h AM was administrated to mice with an ip implanted osmotic pump. Infarct area (A) and blood flow (B) on postoperative d 7 with different starting points for AM administration. *, $P < 0.05$; **, $P < 0.01$; ns, not significant *vs.* vehicle; n = 6.

lature, the so-called "vascular niche" (35), where endothelial cells secrete neurogenic factors, including basic fibroblast growth factor, vascular endothelial growth factor, and brain-derived neurotrophic factor, and create conditions conducive to neurogenesis (36). Therefore, vascular regeneration is assumed to rescue ischemic brain via not only supply of oxygen and nutrition but also promotion of neurogenesis. We confirmed in this study that neurogenesis occurred adjacent to neovessels in the ischemic core and the number of regenerated neurons was correlated with vascular density.

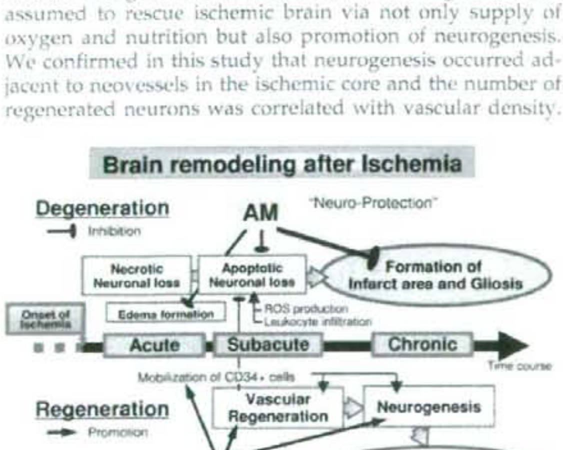

FIG. 10. Summary of brain remodeling after ischemia and effects of AM on the ischemic brain observed in this study.

We have assigned the term "vasculo-neuro-regeneration" to the entire process of enhancement of vasculogenesis and subsequent neurogenesis.

We demonstrated that AM promotes vasculo-neuro-regeneration in the ischemic brain. Blood flow and capillary density in the ischemic brain after 20m-MCAO was significantly enhanced in AM-Tg mice after postoperative d 7 with subsequent promotion of neurogenesis after d 28. The promoted vasculogenesis and neurogenesis observed in AM-Tg mice was significantly correlated with the functional recovery after 20m-MCAO. This result suggests that these two regenerative elements might contribute to the functional recovery after 20m-MCAO. The neovascularization was preceded by augmented mobilization of $CD34^+$ mononuclear cells, which are known to differentiate into endothelial cells and contribute to vasculogenesis (37). Recently, iv infusion of $CD34^+$ cells has reported to promote not only neovascularization but also neurogenesis (38). Furthermore, we observed the direct promoting action of AM on neural differentiation of PC12 cells via cAMP/PKA- and PI3K/Akt-dependent pathways. The totality of these findings suggests that the neurogenic action of AM *in vivo* comprises at least two different mechanisms: a direct action on neuronal cells through activation of PKA and Akt and an indirect action on neurogenesis after enhanced neovascularization.

Judging from the ratio of mature AM to total AM as shown in Table 1, the mature AM concentration in the ischemic brain of AM-Tg mice was expected to be 1~4 fmol/g tissue. The concentration seems to be comparable to the reported effective concentration of mature AM *in vivo* (25, 39). The *in vivo* concentration of human mature AM in the whole brain (1 fmol/g tissue level) and in the plasma (10 fmol/ml level) might be lower than the minimal concentration required for its *in vitro* action (100 fmol/ml) observed in this study. The actual effective concentration *in vitro*, however, might be lower because the administrated peptide is rapidly degradated *in vitro*. In addition, it is demonstrated in previous reports including ours (40, 41), that peptides could exert their significant actions at the stably maintained concentration, that is, by 2 orders of magnitude lower than that of bolus administration. In AM-Tg mice, the AM concentration was maintained at the same level due to the constitutive overproduction by the human serum amyloid P component promoter. Thus, we suppose that the direct neuronal action of AM *in vivo* could be possible in this stroke model.

In view of clinical application, we also tried exogenous administration of AM by ip implanted osmotic pump to determine appropriate amount and timing of AM administration after 20m-MCAO. Previous reports on AM administration for rodents or human set the therapeutic dose at 2~25 fmol/ml (25, 39). For our experiments, therefore, we used two lines of transgenic mice with a plasma concentration of mature AM of 24.9 ± 4.2 and 2.6 ± 0.6 fmol/ml. The results showed comparable effects of AM in these two lines on neuroprotection and vascular regeneration. This led us to conclude that a plasma level of 2~3 fmol/ml of mature AM, 3~5 times higher than its physiological concentration, was sufficient to attain therapeutic effects for the mice after 20m-MCAO. We next tried exogenous infusion of AM with an osmotic pump in the amount reported to achieve a plasma concentration of 2~3 fmol/ml. The exogenous AM treatment which started just after the induction of 20m-MCAO or at 24 h after produced significant effects that were comparable to those seen in the two lines of AM-Tg mice. However, that from 72 h postoperatively failed to reveal significant effects. These results showed that appropriate timing to start AM administration after stroke is less than 72 h after the event.

We performed two different stroke models, nonfatal 20m-MCAO and fatal 2 h-MCAO. In 2 h-MCAO, we observed significant reduction of brain edema in AM-Tg mice through reduction of vascular permeability, which is compatible with previous report (42). However, infarct size was not reduced on postoperative d 1 after 2 h-MCAO. The result suggests that AM exerts more significant therapeutic effect on the brain tissue after nonfatal ischemia. The therapeutic potential for brain edema after fatal stroke is further to be elucidated.

Cerebral ischemia, including stroke, vascular Parkinson's disease and vascular dementia, is one of the most serious medical problems because it causes critical impairment of activity and quality of daily life. Regenerative medicine is now in the spotlight as a promising therapy to treat ischemic brain which has been considered to be irreversible and indicated for no active treatment. Various humoral factors are anticipated for their therapeutic potential for ischemic brain through neurogenic (*e.g.* basic fibroblast growth factor and epidermal growth factor) and angiogenic (*e.g.* vascular endothelial growth factor and hepatocyte growth factor) effects (43–47). Among them, we believe that the vascular hormone AM has several advantages as a therapeutic agent for ischemic brain. We can expect multiple effects of AM through its neuroprotective and vasculo-neuro-regenerative actions as shown in this study. In addition, AM has already been safely used for human patients with heart failure or pulmonary hypertension without any mention of critical adverse effects resulting from iv administration (39).

Thus, we are prompted to propose a new strategy to rescue ischemic brain by using vascular hormone AM for the combined neuroprotective and vasculo-neuro-regenerative therapy to improve impaired neurological function.

Acknowledgments

This work was supported by grants from Japanese ministry of Education, Culture, Sports, Science and Technology; ministry of Health, Labor and Welfare; and University of Kyoto 21st Century Centers of Excellence program. We thank Dr. Seiichi Hashida (Department of Biochemistry, University of Miyazaki) for measuring mature PAMP; and Dr. Kazuhiko Nozaki and Masaki Nishimura, (Department of Neurosurgery, University of Kyoto) for technical assistance.

Received August 15, 2005. Accepted December 19, 2005.

Address all correspondence and requests for reprints to: Hiroshi Itoh, M.D., Ph.D., Department of Medicine and Clinical Science, Kyoto University Graduate School of Medicine; 54 Shogoin Kawahara-cho, Sakyo-ku, Kyoto 606-8507, Japan. E-mail: hiito@kuhp.kyoto-u.ac.jp.

This work was supported by Japanese ministry of Education, Culture, Sports, Science and Technology; ministry of Health, Labor and Welfare; and University of Kyoto 21st Century Centers of Excellence program.

References

1. **Kitamura K, Kangawa K, Kawamoto M, Ichiki Y, Nakamura S, Matsuo H, Eto T** 1993 Adrenomedullin: a novel hypotensive peptide isolated from human pheochromocytoma. Biochem Biophys Res Commun 92:553–560
2. **Nagaya N, Mori H, Murakami S, Kangawa K, Kitamura S** 2005 Adrenomedullin: angiogenesis and gene therapy. Am J Physiol Regul Integr Comp Physiol 288:R1432–R1437
3. **Shindo T, Kurihara Y, Nishimatsu H, Moriyama N, Kakoki M, Wang Y, Imai Y, Ebihara A, Kuwaki T, Ju KH, Minamino N, Kangawa K, Ishikawa T, Fukuda M, Akimoto Y, Kawakami H, Imai T, Morita H, Yazaki Y, Nagai R, Hirata Y, Kurihara H** 2001 Vascular abnormalities and elevated blood pressure in mice lacking adrenomedullin gene. Circulation 104:1964–1971
4. **Shimosawa T, Shibagaki Y, Ishibashi K, Kitamura K, Kangawa K, Kato S, Ando K, Fujita T** 2002 Adrenomedullin, an endogenous peptide, counteracts cardiovascular damage. Circulation 105:106–111
5. **Imai Y, Shindo T, Maemura K, Sata M, Saito Y, Kurihara Y, Akishita M, Osuga J, Ishibashi S, Tobe K, Morita H, Oh-hashi Y, Suzuki T, Maekawa H, Kangawa K, Minamino N, Yazaki Y, Nagai R, Kurihara H** 2002 Resistance to neointimal hyperplasia and fatty streak formation in mice with adrenomedullin overexpression. Arterioscler Thromb Vasc Biol 22:1310–1315
6. **Miyashita K, Itoh H, Sawada N, Fukunaga Y, Sone M, Yamahara K, Yurugi-Kobayashi T, Park K, Nakao K** 2003 Adrenomedullin provokes endothelial Akt activation and promotes vascular regeneration both in vitro and in vivo. FEBS Lett 544:86–92
7. **Miyashita K, Itoh H, Sawada N, Fukunaga Y, Sone M, Yamahara K, Yurugi T, Nakao K** 2003 Adrenomedullin promotes proliferation and migration of cultured endothelial cells. Hypertens Res 26:S93–S98
8. **Abe M, Sata M, Nishimatsu H, Nagata D, Suzuki E, Terauchi Y, Kadowaki T, Minamino N, Kangawa K, Matsuo H, Hirata Y, Nagai R** 2003 Adrenomedullin augments collateral development in response to acute ischemia. Biochem Biophys Res Commun 306:10–15
9. **Kim W, Moon SO, Sung MJ, Kim SH, Lee S, So JN, Park SK** 2003 Angiogenic role of adrenomedullin through activation of Akt, mitogen-activated protein kinase, and focal adhesion kinase in endothelial cells. FASEB J 17:1937–1939
10. **Tokunaga N, Nagaya N, Shirai M, Tanaka E, Ishibashi-Ueda H, Harada-Shiba M, Kanda M, Ito T, Shimizu W, Tabata Y, Uematsu M, Nishigami K, Sano S, Kangawa K, Mori H** 2004 Adrenomedullin gene transfer induces therapeutic angiogenesis in a rabbit model of chronic hind limb ischemia: benefits of a novel nonviral vector, gelatin. Circulation 109:526–531
11. **Iwase T, Nagaya N, Fujii T, Itoh T, Ishibashi-Ueda H, Yamagishi M, Miyatake K, Matsumoto T, Kitamura S, Kangawa K** 2005 Adrenomedullin enhances angiogenic potency of bone marrow transplantation in a rat model of hindlimb ischemia. Circulation 111:356–362
12. **Eto T** 2001 A review of the biological properties and clinical implications of adrenomedullin and proadrenomedullin N-terminal 20 peptide (PAMP), hypotensive and vasodilating peptides. Peptides 22:1693–1711
13. **Serrano J, Alonso D, Fernandez AP, Encinas JM, Lopez JC, Castro-Blanco S, Fernandez-Vizarra P, Richart A, Santacana M, Uttenthal LO, Bentura ML, Martinez-Murillo R, Martinez A, Cuttitta F, Rodrigo J** 2002 Adrenomedullin in the central nervous system. Microsc Res Tech 57:76–90
14. **Wang X, Yue TL, Barone FC, White RF, Clark RK, Willette RN, Sulpizio AC, Aiyar NV, Ruffolo Jr RR, Feuerstein GZ** 1995 Discovery of adrenomedullin in rat ischemic cortex and evidence for its role in exacerbating focal brain ischemic damage. Proc Natl Acad Sci USA 92:11480–11484
15. **Dogan A, Suzuki Y, Koketsu N, Osuka K, Saito K, Takayasu M, Shibuya M, Yoshida J** 1997 Intravenous infusion of adrenomedullin and increase in regional cerebral blood flow and prevention of ischemic brain injury after middle cerebral artery occlusion in rats. J Cereb Blood Flow Metab 17:19–25
16. **Watanabe K, Takayasu M, Noda A, Hara M, Takagi T, Suzuki Y, Yoshia J** 2001 Adrenomedullin reduces ischemic brain injury after transient middle cerebral artery occlusion in rats. Acta Neurochir (Wien) 143:1157–1161
17. **Xia CF, Yin H, Borlongan CV, Chao J, Chao L** 2004 Adrenomedullin gene delivery protects against cerebral ischemic injury by promoting astrocyte migration and survival. Hum Gene Ther 15:1243–1254
18. **Hashida S, Kitamura K, Nagatomo Y, Shibata Y, Imamura T, Yamada K, Fujimoto S, Kato J, Morishita K, Eto T** 2004 Development of an ultrasensitive enzyme immunoassay for human proadrenomedullin N-terminal 20 peptide and direct measurement of two molecular forms of PAMP in plasma from healthy subjects and patients with cardiovascular disease. Clin Biochem 37:14–21
19. **Longa EZ, Weinstein PR, Carlson S, Cummins R** 1989 Reversible middle cerebral artery occlusion without craniectomy in rats. Stroke 20:84–91
20. **Teramoto T, Qiu J, Plumier JC, Moskowitz MA** 2003 EGF amplifies the replacement of parvalbumin-expressing striatal interneurons after ischemia. J Clin Invest 111:1125–1132
21. **Venditti A, Battaglia A, Del Poeta G, Buccisano F, Maurillo L, Tamburini A, Del Moro B, Epiceno AM, Martiradonna M, Caravita T, Santinelli S, Adorno G, Picardi A, Zinno F, Lanti A, Bruno A, Suppo G, Franchi A, Franconi G, Amadori S** 1999 Enumeration of CD34+ hematopoietic progenitor cells for clinical transplantation: comparison of three different methods. Bone Marrow Transplant 24:1019–1027
22. **Swanson RA, Morton MT, Tsao-Wu G, Savalos RA, Davidson C, Sharp FR** 1990 A semiautomated method for measuring brain infarct volume. J Cereb Blood Flow Metab 10:290–293
23. **Zhang ZG, Zhang L, Croll SD, Chopp M** 2002 Angiopoietin-1 reduces cerebral blood vessel leakage and ischemic lesion volume after focal cerebral embolic ischemia in mice. Neuroscience 2002 113:683–687

24. **Hayashi H, Ishisaki A, Imamura T** 2003 Smad mediates BMP-2-induced upregulation of FGF-evoked PC12 cell differentiation. FEBS Lett 536:30–34
25. **Iimuro S, Shindo T, Moriyama N, Amaki T, Niu P, Takeda N, Iwata H, Zhang Y, Ebihara A, Nagai R** 2004 Angiogenic effects of adrenomedullin in ischemia and tumor growth. Circ Res 95:415–423
26. **Nakano S, Kogure K, Fujikura H** 1990 Ischemia-induced slowly progressive neuronal damage in the rat brain. Neuroscience 38:115–124
27. **Graham SH, Chen J** 2001 Programmed cell death in cerebral ischemia. J Cereb Blood Flow Metab 21:99–109
28. **Northington FJ, Ferriero DM, Graham EM, Traystman RJ, Martin LJ** 2001 Early neurodegeneration after hypoxia-ischemia in neonatal rat is necrosis while delayed neuronal death is apoptosis. Neurobiol Dis 8:207–219
29. **Stoll G, Jander S, Schroeter M** 1998 Inflammation and glial responses in ischemic brain lesions. Prog Neurobiol 56:149–171
30. **Gilgun-Sherki Y, Rosenbaum Z, Melamed E, Offen D** 2002 Antioxidant therapy in acute central nervous system injury: current state. Pharmacol Rev 54:271–284
31. **Kim W, Moon SO, Lee S, Sung MJ, Kim SH, Park SK** 2003 Adrenomedullin reduces VEGF-induced endothelial adhesion molecules and adhesiveness through a phosphatidylinositol 3'-kinase pathway. Arterioscler Thromb Vasc Biol 23:1377–1383
32. **Kawai J, Ando K, Tojo A, Shimosawa T, Takahashi K, Onozato ML, Yamasaki M, Ogita T, Nakaoka T, Fujita T** 2004 Endogenous adrenomedullin protects against vascular response to injury in mice. Circulation 109:1147–1153
33. **Niu P, Shindo T, Iwata H, Iimuro S, Takeda N, Zhang Y, Ebihara A, Suematsu Y, Kangawa K, Hirata Y, Nagai R** 2004 Protective effects of endogenous adrenomedullin on cardiac hypertrophy, fibrosis, and renal damage. Circulation 109:1789–1794
34. **Krupinski J, Kaluza J, Kumar P, Kumar S, Wang JM** 1994 Role of angiogenesis in patients with cerebral ischemic stroke. Stroke 25:1794–1798
35. **Palmer TD, Willhoite AR, Gage FH** 2000 Vascular niche for adult hippocampal neurogenesis. J Comp Neurol 425:479–494
36. **Louissaint Jr A, Rao S, Leventhal C, Goldman SA** 2002 Coordinated interaction of neurogenesis and angiogenesis in the adult songbird brain. Neuron 34:945–960
37. **Asahara T, Murohara T, Sullivan A, Silver M, van der Zee R, Li T, Witzenbichler B, Schatteman G, Isner JM** 1997 Isolation of putative progenitor endothelial cells for angiogenesis. Science 275:964–967
38. **Taguchi A, Soma T, Tanaka H, Kanda T, Nishimura H, Yoshikawa H, Tsukamoto Y, Iso H, Fujimori Y, Stern DM, Naritomi H, Matsuyama T** 2004 Administration of CD34+ cells after stroke enhances neurogenesis via angiogenesis in a mouse model. J Clin Invest 114:330–338
39. **Nagaya N, Satoh T, Nishikimi T, Uematsu M, Furuichi S, Sakamaki F, Oya H, Kyotani S, Nakanishi N, Goto Y, Masuda Y, Miyatake K, Kangawa K** 2000 Hemodynamic, renal, and hormonal effects of adrenomedullin infusion in patients with congestive heart failure. Circulation 101:498–503
40. **Doi K, Itoh H, Ikeda T, Hosoda K, Ogawa Y, Igaki T, Yamashita J, Chun TH, Inoue M, Masatsugu K, Matsuda K, Ohmori K, Nakao K** 1997 Adenovirus-mediated gene transfer of C-type natriuretic peptide causes G1 growth inhibition of cultured vascular smooth muscle cells. Biochem Biophys Res Commun 239:889–894
41. **Komatsu Y, Itoh H, Suga S, Ogawa Y, Hama N, Kishimoto I, Nakagawa O, Igaki T, Doi K, Yoshimasa T, Nakao K** 1996 Regulation of endothelial production of C-type natriuretic peptide in coculture with vascular smooth muscle cells. Role of the vascular natriuretic peptide system in vascular growth inhibition. Circ Res 78:606–614
42. **Hippenstiel S, Witzenrath M, Schmeck B, Hocke A, Krisp M, Krull M, Seybold J, Seeger W, Rascher W, Schutte H, Suttorp N** 2002 Adrenomedullin reduces endothelial hyperpermeability. Circ Res 91:618–625
43. **Nakatomi H, Kuriu T, Okabe S, Yamamoto S, Hatano O, Kawahara N, Tamura A, Kirino T, Nakafuku M** 2002 Regeneration of hippocampal pyramidal neurons after ischemic brain injury by recruitment of endogenous neural progenitors. Cell 110:429–441
44. **Zhang ZG, Zhang L, Jiang Q, Zhang R, Davies K, Powers C, Bruggen N, Chopp M** 2000 VEGF enhances angiogenesis and promotes blood-brain barrier leakage in the ischemic brain. J Clin Invest 106:829–838
45. **Shimamura M, Sato N, Oshima K, Aoki M, Kurinami H, Waguri S, Uchiyama Y, Ogihara T, Kaneda Y, Morishita R** 2004 Novel therapeutic strategy to treat brain ischemia: overexpression of hepatocyte growth factor gene reduced ischemic injury without cerebral edema in rat model. Circulation 109:424–431
46. **Sun Y, Jin K, Xie L, Childs J, Mao XO, Logvinova A, Greenberg DA** 2003 VEGF-induced neuroprotection, neurogenesis, and angiogenesis after focal cerebral ischemia. J Clin Invest 111:1843–1851
47. **Sondell M, Lundborg G, Kanje M** 1999 Vascular endothelial growth factor has neurotrophic activity and stimulates axonal outgrowth, enhancing cell survival and Schwann cell proliferation in the peripheral nervous system. J Neurosci 19:5731–5740

Endocrinology is published monthly by The Endocrine Society (http://www.endo-society.org), the foremost professional society serving the endocrine community.

Selective Impairment of Working Memory in a Mouse Model of Chronic Cerebral Hypoperfusion

Masunari Shibata, MD; Nobuyuki Yamasaki, MD; Tsuyoshi Miyakawa, PhD; Rajesh N. Kalaria, PhD, FRCPath; Youshi Fujita, MD; Ryo Ohtani, MD; Masafumi Ihara, MD; Ryosuke Takahashi, MD; Hidekazu Tomimoto, MD

Background and Purpose—We recently designed a mouse model of chronic cerebral hypoperfusion, in which the cerebral white matter is damaged without significant gray matter lesions. The behavioral characteristics of these mice were studied using a test battery for neurological and cognitive functions.

Methods—Adult C57Bl/6 male mice were subjected to either sham-operation or bilateral common carotid artery stenosis (BCAS) using microcoils with an internal diameter of 0.18 mm. At 30 days after BCAS, 70 animals were divided into 3 groups and subjected to behavioral test batteries. The first group underwent comprehensive behavioral test, including the neurological screen, prepulse inhibition, hot plate, open field, light/dark transition, Porsolt forced swim and contextual and cued fear conditioning (BCAS $n=13$; sham-operated $n=11$). The second group was for the working memory task of the 8-arm radial maze test (BCAS $n=12$; sham-operated $n=10$), and the third for the reference memory task of the 8-arm radial maze test (BCAS $n=13$; sham-operated $n=11$). Another batch of animals were examined for histological changes (BCAS $n=11$; sham-operated $n=12$).

Results—The white matter including the corpus callosum was consistently found to be rarefied without clear ischemic lesions in the hippocampus. No apparent differences were observed in the comprehensive test batteries between the control and BCAS mice. However, in the working memory tasks tested with the 8-arm radial maze, the BCAS mice made significantly more errors than the control mice ($P<0.0001$). Again, there were no detectable differences in the reference memory tasks between the groups.

Conclusions—At 30 days after BCAS, working memory deficits as well as white matter changes were apparent in the mice. Working memory deficit was attributable to damage of the frontal-subcortical circuits, suggesting the BCAS model is useful to evaluate the substrates of subcortical vascular dementia. **(*Stroke*. 2007;38:2826-2832.)**

Key Words: behavioral neurology ■ cerebral blood flow ■ hippocampus ■ leukoaraiosis ■ memory ■ vascular dementia ■ white matter disease

Cerebral blood flow (CBF) is decreased in patients with vascular dementia. Subcortical vascular dementia, the major subtype of vascular dementia, is featured by small vessel disease involving white matter (WM) changes and lacunar infarctions. Arteriosclerosis may induce these WM lesions after longstanding cerebral hypoperfusion.[1] In support for this hypothesis, hypoxia-inducible factor-1 is expressed in cerebrovascular WM lesions.[2] In addition, WM lesions are observed in rodent models of chronic cerebral hypoperfusion, in which the bilateral carotid arteries are stenosed or ligated,[3–7] and stroke-prone spontaneously hypertensive rats which have small vessel pathology.[8] Such WM lesions are suggested to contribute to frontal hypometabolism and executive dysfunction.[9,10]

We recently designed a mouse model of chronic cerebral hypoperfusion[11] by placing microcoils bilaterally on the common carotid arteries. These mice invariably exhibited WM changes and have several advantages over other models of chronic cerebral hypoperfusion in rats and gerbils.[3–5,12–14] First, genetically modulated mice produced to model various diseases can be used.[15] Second, the visual pathway is preserved as compared with the rat model, because blood flow in the common carotid arteries albeit reduced is maintained. Third, the cerebral WM is selectively damaged, yet sparing the gray matter such as the hippocampus if the degree of stenosis is appropriately controlled by adjusting the internal diameter of the microcoils.[11]

Received April 4, 2007; accepted April 18, 2007.

From the Department of Neurology (M.S., Y.F., R.O., M.I., R.T., H.T.), Graduate School of Medicine, and Horizontal Brain Research Organization (N.Y., T.M.), Kyoto University, Sakyo-ku, Kyoto, Japan; and the Institute for Health and Ageing (R.N.K.), University of Newcastle upon Tyne, Newcastle General Hospital, Newcastle-upon-Tyne, UK.

Correspondence to Hidekazu Tomimoto, MD, Department of Neurology, Graduate School of Medicine, Kyoto University, Sakyo-ku, Kyoto 606-8507, Japan. E-mail tomimoto@kuhp.kyoto-u.ac.jp

Stroke is available at http://stroke.ahajournals.org DOI: 10.1161/STROKEAHA.107.490151

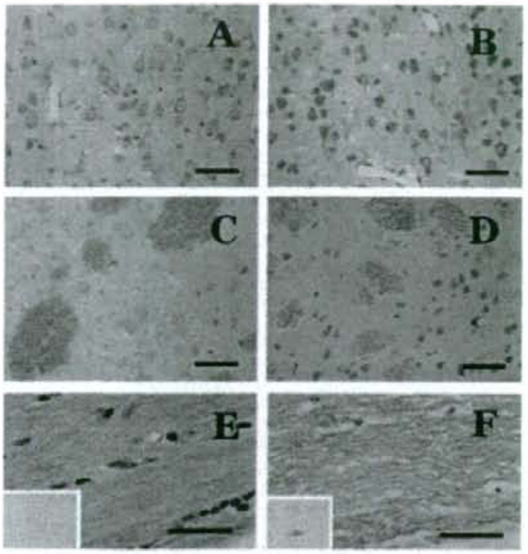

Figure 1. Photomicrographs of Klüver-Barrera staining (A through H) and TUNEL (insets in E and F) in the cerebral cortex (A and B), caudoputamen (C and D), corpus callosum (E and F) and hippocampus (G and H). The left column (A, C, E, and G) indicates the brain from a sham-operated mouse and the right column (B, D, F, and H) indicates a brain after BCAS for 30 days. Note marked vacuoles (F), and intact pyramidal neurons (H) after BCAS. Bars indicate 100 μm (C through F).

In the present study, we used various paradigms to test behavior including working and reference memories in this bilateral carotid artery stenosis (BCAS) mice model of chronic cerebral hypoperfusion. The BCAS model would be useful to explore behavioral substrates of the frontal-subcortical circuit deficits apparent in subcortical vascular dementia.

Materials and Methods

Animals and Experimental Design

Male C57Bl/6 mice (10 to 12 weeks old, 24 to 29 g; Shizuoka laboratory animal center, Hamamatsu) were anesthetized with sodium pentobarbital. Through a midline cervical incision, both common carotid arteries were exposed. A microcoil with a diameter of 0.18 mm was applied to the bilateral common carotid artery, maintaining the rectal temperature between 36.5°C and 37.5°C. Those in the control group were sham-operated, which involved bilateral exposure of the common carotid arteries. The animals were kept in cages for 30 days with food and water ad libitum.

Twenty four mice were examined for histological changes. After BCAS, CBF was measured by laser-Doppler flowmetry at 1, 7 and 30 days, as described previously.[11] These mice were deeply anesthetized with sodium pentobarbital and were perfused transcardially with 0.01 mol/L phosphate-buffered saline (PBS) and then with a fixative containing 4% paraformaldehyde and 0.2% picric acid in 0.1 mol/L phosphate buffer (PB, pH 7.4). The brains were postfixed in 4% paraformaldehyde in 0.1 mol/L PB, and were stored in 20% sucrose in 0.1 mol/L PB (pH 7.4). The brains were then embedded in paraffin and sliced into 6 μm-thick coronal sections. Sequential sections from every 50 to 100 sections were stained with Klüver-Barrera (KB) and hematoxylin and eosin (H&E) stains. TUNEL staining was done using Apoptag in situ kit obtained from Oncor. The WM changes were evaluated specifically in 4 regions: the optic tract, internal capsule, fiber bundles of the caudoputamen, and corpus callosum. In the coronal plane 0.15 mm anterior to the bregma, the areas of right hemisphere and ventricular space 30 days after the operation were digitized using the NIH image analyzer program, and used as an index of brain atrophy.

Another 70 animals, which were 14 to 16 weeks old were divided into 3 groups and examined 30 days after the operation. The first group of the mice was subjected to a comprehensive behavioral test battery.[16,17] The battery included the neurological screen, light/dark transition, open field, hot plate, prepulse inhibition and Porsolt forced swim, contextual and cued fear conditioning, which were conducted in this sequence, with each test separated at least by 1 day (BCAS mice, n=13; sham-operated, n=11). The second group was tested for the working memory task of the 8-arm radial maze (BCAS mice, n=12; sham-operated, n=10), and the third group for the reference memory task (BCAS mice, n=13; sham-operated, n=11).

The mice were housed in a room with a 12-hour light/dark cycle (lights on at 7:00 AM) with access to food and water ad libitum. All procedures were performed according to the guidelines of the Animal Use and Care Committee of Kyoto University.

Neurological Screen

A neurological screen was conducted as previously described.[17] The ear twitch, whisker touch and righting reflexes were evaluated.

Startle Response/Prepulse Inhibition Tests

A startle reflex measurement system was used (O'Hara & Co). The test session began by placing a mouse in a plexiglasss cylinder for 10 minutes. The duration of white noise as the startle stimulus was 40 ms for all trial types. The startle response was recorded for 140 ms (measuring the response every 1 ms) starting with the onset of the prepulse stimulus. The peak startle amplitude recorded during the 140-ms sampling window was used as the dependent variable. A test session consisted of 6 trial types (ie, 2 types for startle stimulus only trials, and 4 types for prepulse inhibition trials). The intensity of startle stimulus was 110 or 120 dB. The prepulse sound was presented 100 ms before the startle stimulus, and its intensity was 74 or 78 dB. Four combinations of prepulse and startle stimuli were used (74/110, 78/110, 74/120, and 78/120). Six blocks of the 6 trial types were presented in pseudorandom order such that each trial type was presented once within a block. The average intertrial interval was 15 s (range: 10 to 20 s).

Hot Plate Test

The hotplate test for nociception was used to evaluate sensitivity to a thermal stimulus. Mice were placed on a 55.0 (±0.3)°C hot plate (Columbus Instruments), and latency to the first hind-paw response (a foot shake or a paw lick) was recorded.

Motor Function Tests

Motor coordination and balance were tested with the rotarod test, and neuromuscular strength was tested with wire hang test and grip strength test.[17] In the wire hang test, the mouse was placed on a wire cage lid apparatus (O'hara & Co) to assess balance and grip strength. The mouse was placed on a wire mesh, which was then inverted, and latency to fall was recorded. A grip strength meter (O'hara & Co) was used to assess forelimb grip strength, when mice were pulled back. The rotarod test was performed by placing a mouse on a rotating drum (UGO Basile Accelerating Rotarod), and the time to maintain its balance on the rod was measured. The speed of the rotarod was accelerated from 4 to 40 rpm over a 5-minute period.

Table. General Physical Characteristics and Sensory/Motor Functions of BCAS Mice and Sham-Operated Mice

	BCAS	Sham	*P* Value
Physical characteristics			
Age, wk	14.1	14.1	
Whiskers, % with	100	100	
Fur, % with normal fur	100	100	
Rectal temperature, °C	36.9 (±0.1)	37.0 (±0.1)	$F_{1,22}$=0.495, *P*=0.4893
Sensory motor reflex			
Ear twitch, % with quick response	100	100	
Whisker twitch, % with normal response	100	100	
Righting reflex, % with normal response	100	100	
Acoustic startle response, arbitrary unit			
Stimulus intensity=110 dB	1.2 (±0.1)	1.3 (±0.2)	$F_{1,21}$=0.042, *P*=0.8393
Stimulus intensity=120 dB	1.8 (±0.2)	1.9 (±0.3)	$F_{1,21}$=0.094, *P*=0.762
Prepulse inhibition (%; stimulus=110 dB)			
Prepulse intensity=74 dB	42.2 (±8.0)	22.3 (±6.7)	$F_{1,21}$=3.566, *P*=0.0729
Prepulse intensity=78 dB	61.7 (±6.0)	48.9 (±4.0)	$F_{1,21}$=3.026, *P*=0.0966
Prepulse inhibition (%; stimulus=120 dB)			
Prepulse intensity=74 dB	31.1 (±10.4)	23.6 (±7.0)	$F_{1,21}$=0.342, *P*=0.5651
Prepulse intensity=78 dB	50.7 (±7.6)	44.2 (±5.6)	$F_{1,21}$=0.465, *P*=0.5027
Pain test			
Hot plate test (latency; s)	7.7 (±0.6)	7.6 (±0.6)	$F_{1,22}$=0.003, *P*=0.9548
Motor test			
Wire hang (latency to fall; s)	51.1 (±4.0)	60.0 (±0.0)	$F_{1,22}$=4.108, *P*=0.055
Grip strength (N)	0.83 (±0.04)	0.81 (±0.04)	$F_{1,22}$=0.266, *P*=0.611
Rotarod (latency to fall; s; average of 3 trials)			
Day 1	137 (±13)	167 (±14)	$F_{1,22}$=2.254, *P*=0.1475
Day 2	201 (±17)	226 (±13)	$F_{1,22}$=1.274, *P*=0.2712

Data represent the mean (±SEM; BCAS, n=13; sham, n=11).

Open Field Test

Locomotor activity was measured using an open field test. Each subject was placed in the center of the open field apparatus (40×40×30 cm; Accuscan Instruments). Total distance traveled (in cm), vertical activity (rearing measured by counting the number of photobeam interruptions), time spent in the center, and the beam-break counts for stereotyped behavior (stereotypic counts) were recorded. Data were collected for 120 minutes.

Light/Dark Transition Test

The apparatus used for the light/dark transition test consisted of a cage (21×42×25 cm) divided into 2 chambers, one of which was brightly illuminated (390 lux), and the other was dark (2 lux). Mice were placed into the dark side and allowed to move freely for 10 minutes. The total number of transitions, time spent in each side, first latency to light side, and distance traveled were recorded by Image LD software (see 'Image Analysis').

Porsolt Forced Swim Test

In the Porsolt forced swim test, the apparatus consisted of 4 plexiglass cylinders (20 cm height ×10 cm diameter). The cylinders were filled with water (23°C), up to a height of 7.5 cm. Mice were placed into the cylinders, and their behavior was recorded over a 10-minute test period (day 1, 2). Data acquisition and analysis were performed automatically, using Image PS software (see 'Image Analysis').

Contextual and Cued Fear Conditioning

Each mouse was placed in a test chamber (26×34×33 cm; O'hara & Co) and allowed to explore freely for 2 minutes. A 55-dB white noise, which served as the conditioned stimulus, was presented for 30 s, followed by a mild (2 s, 0.3 mA) footshock, which served as the unconditioned stimulus. Two more conditioned stimulus–unconditioned stimulus pairings were presented with 2-minute interstimulus interval. Context testing was conducted 24 hours after conditioning in the same chamber. Cued testing with altered context was conducted 24 hours after conditioning using a triangular box (35×35×41 cm), which was located in a different room.

Data acquisition, control of stimuli, and data analysis were performed automatically, using Image FZ software (see 'Image Analysis'). Images were captured at 1 frame per second. For each pair of successive frames, the amount of area (pixels) by which the mouse moved was measured. When this area was below a certain threshold (ie, 20 pixels), the behavior was judged as 'freezing'. The optimal threshold (amount of pixels) to judge freezing was determined by adjusting it to the amount of freezing measured by human observation.

Eight-Arm Radial Maze Test

The 8-arm radial maze test was conducted as described previously.[17] Each arm (9×40 cm) radiated from an octagonal central starting platform. Identical food wells with pellet sensors were placed at the distal end of each arm. As the initial pretraining, each mouse was placed in the central starting platform and allowed to explore and to consume food pellets scattered on the whole maze for a 5-minute period. Subsequently, these mice received another pretraining to take a pellet from each food well after being placed at the distal end of each arm. A trial was finished after the subject consumed the pellet. This was repeated 8 times, using 8 different arms, for each mouse.